AN ABSTRACT OF THE THESIS OF

Gabriel García-Medina for the degree of Master of Science in Civil Engineering presented on September 7, 2012.

Title: Nearshore Wave Predictions along the Oregon and Southwest Washington Coast

Abstract approved:

_____

H. Tuba Özkan-Haller

This thesis contains a manuscript describing the implementation of a high resolution wave forecasting model for the coasts of Washington and Oregon. The purpose of this project was to advance the wave predictive capabilities of the states of Oregon and the southwest part of Washington by including the effects of local bathymetric features in the operational forecasts. A 30 arc-second resolution wave forecasting model was implemented making use of the WAVEWATCH III numerical code covering the coastal region from Klamath, CA to Taholah, WA. The wave forecasts extend to the continental shelf at this resolution. To assess the performance of the model, its output was compared against *in situ* data, with normalized root-mean-squared errors in significant wave height in the vicinity of 0.20 and linear correlation coefficients greater than 0.80. Making use of the resulting validated regional scale wave forecasting system, an evaluation of the model sensitivity to the inclusion of bottom friction and wind input at the shelf level was performed. Results suggest that neither dissipation due to bottom friction or wind generation are significant for long term forecasting/hindcasting in the region. Results from a series of hindcasts suggest that several significant offshore features may affect the nearshore wave field. To evaluate it, a shelf scale SWAN model was implemented and a series of numerical experiments performed. Results suggest that the Astoria and McArthur Canyons; the Stonewall,

Perpetua, and Heceta Banks; and Cape Blanco are significant bathymetric features that are capable of producing significant alongshore variability in wave heights nearshore.

Nearshore Wave Predictions along the Oregon and Southwest Washington Coast

by

Gabriel García-Medina

A THESIS

submitted to

Oregon State University

in partial fulfillment of

the requirements for the

degree of

Master of Science

Presented September 7, 2012

Commencement June 2013

Master of Science thesis of Gabriel García-Medina presented on September 7, 2012.

APPROVED:

_____

Major Professor, representing Civil and Construction Engineering

_____

Head of the School of Civil and Construction Engineering

_____

Dean of the Graduate School

I understand that my thesis will become part of the permanent collection of Oregon State University libraries. My signature below authorizes release of my thesis to any reader upon request.

_____

Gabriel García-Medina, Author

ACKNOWLEDGEMENTS

I want to thank my advisor Dr. H. Tuba Özkan-Haller for her immeasurable contributions to my growth as a professional and more importantly as a person. Thanks for all the time you spent teaching me science, writing, public speaking, etc. I have really enjoyed the experience of working together.

I would also like to thank Dr. Peter Ruggiero for the interesting discussions about coastal processes and for sharing his endless research ideas and questions. Also, thank you for teaching me some of the mysteries of the English language. I want to thank Dr. Merrick Haller for his helpful contributions to the projects I worked in and for accepting my late application to the MS program.

I want to thank my office mates Jeffrey Oskamp, Gregory Wilson, and Sarah Kassem for their helpful conversations. Also want to thank Cameron McNatt, Cássia Pianca, Katy Serafin, Adam Keen, Kyle Landon, John Stanley, and Dr. Rob Holman for their support and fun times we had together. I want to thank my friends in Corvallis for their support and making me feel at home 6,000 km away from San Juan.

The work presented in this thesis was supported by Oregon Sea Grant under Award Number NA10OAR4170059 and by the United States Department of Energy under Award Number DE-FG36-08G018179. Neither the United States Government nor any agency thereof, nor any of their employees, makes any warranty, expressed or implied, or assumes any legal liability or responsibility for the accuracy, completeness, or usefulness of any information, apparatus, produce, or process disclosed, or represents that its use would not infringe upon privately owned rights. Reference herein to any specific commercial product, process, or service by trade name, trademark, manufacturer, or otherwise does not necessarily constitute or imply its endorsement, recommendation, or favoring by the United States Government or any agency thereof. The views and opinions of the authors expressed herein do not necessarily state or reflect those of the United States Government or any agency thereof.

CONTRIBUTION OF AUTHORS

Dr. Peter Ruggiero was the co-principal investigator of the project, contributed with data, ideas and editing. Jeffrey Oskamp's work as a graduate student in the Ocean Engineering program was the first to suggest that bottom friction and wind input were not important for long term wave modeling in the Pacific Northwest region of the United States of America, this was further investigated in the work presented here.

TABLE OF CONTENTS

LIST OF FIGURES

LIST OF TABLES

Table Page

NEARSHORE WAVE PREDICTIONS ALONG THE OREGON AND SOUTHWEST WASHINGTON COAST

1 General Introduction

The Pacific Northwest Coast of the United States of America (i.e. Washington, Oregon and Northern California) is known to be one of the most beautiful in the world. U. S. Route 101, extending from Los Angeles, CA to Sappho, WA, provides easy access to the beaches, coastal forests, dunes, and headlands. Hundreds of thousands of visitors enjoy the various activities these coasts have to offer, such as surfing, fishing, whale watching, and swimming, among others. This coast is one of the most popular destinations in the region. In addition, this region has one of the most severe wave climates in the northern hemisphere with at least one annual significant wave height (SWH) event exceeding 10m in deep water (Ruggiero et al. 2010), with the largest recorded significant wave height being around 15m (Allan and Komar, 2006). This rather extreme wave climate is coupled with recent evidence of a multi-decadal increase in SWH (Allan and Komar, 2000, 2006; Komar et al. 2009; Menéndez et al., 2008; Ruggiero et al., 2010; Seymour, 2011; Young et al., 2011). Since 2000, this wave height increase has been well documented. Allan and Komar (2000) suggested that SWHs at 275 nautical miles west of Coos Bay, Oregon have been increasing at a yearly rate of 0.013 m/yr. More recent publications report an annual increase of 0.010 m/yr (Ruggiero et al. 2010) with larger rates for the annual maximum event, suggesting that bigger waves are increasing at a higher rate. As more data is acquired and the methods fine-tuned, these estimates change; but the increasing trend is consistent. These combinations of factors produce potentially hazardous conditions for navigation and ocean users in general. Thus, detailed knowledge of the wave conditions is needed.

Recently, harvesting renewable energy has gained much ground. Among these, marine energy, in particular, wave energy is in its early stages of development and gaining much attention from the scientific and industrial communities. In the state of

Oregon, there has been interest in reducing the carbon footprint of the state. One of the goals of the Oregon Wave Energy Trust is to power two Oregon communities with marine energy by 2025. The PNW has been identified as a suitable location for wave energy harvesting, both due to the suitable wave energy resource and modern infrastructure. Arinaga and Cheung (2012) have quantified the winter swell wave power from a 10-year hindcast as 37 KW/h. Lenee-Bluhm et al. (2011) analyzed the wave energy resource in the region from buoy measurements, and found that over most of the PNW at least 5/6 of the waves have SWH in the excess of 1 meter. Incidentally, the normal operation range for the Ocean Power Technologies PB150 Power Buoy is in the range of 1-6 m SWH. Nevertheless, since the power output of these devices is dependent on the wave conditions, a detailed localized knowledge of the future wave conditions is desired.

Due to its high economic costs, it is not possible to measure the wave conditions in detail on this coast. Currently only 7 buoys are in operation in the continental shelf offshore Oregon, USA. The United States Government operates a wave forecasting model covering the whole of the US coastlines (http://polar.ncep.noaa.gov/waves/). These forecasts are produced at a resolution that is not good enough to account for the potential effects of local bathymetric features such as canyons, banks and shoals with length scales of 20km. The PNW is characterized by having a complex bathymetry with features like the Astoria Canyon, Heceta Bank and Cape Blanco which have the potential of affecting the nearshore wave field. Their inclusion in operational forecasts may significantly improve the representation of the wave field in this region and enhance our understanding of the dominant wave transformation processes in play in the PNW.

To satisfy these needs, and other potential ones such as coastal flood forecasting, a high resolution operational wave forecasting model was implemented in this region. In this document, the implementation, validation and operational products are discussed. Also, sensitivity analyses as well as a characterization of the wave behavior in the region are presented.

2 A Nearshore Wave Forecasting System for the US Pacific Northwest

Gabriel García-Medina, H. Tuba Özkan-Haller
Peter Ruggiero, Jeffrey Oskamp

Weather and Forecasting
45 Beacon Street
Boston, MA 02108-3693
Submitted June 2012

Abstract

An operational nearshore wave forecasting system was implemented for the Oregon and southwest Washington coast in the U.S. Pacific Northwest (PNW). High resolution wave forecasts are useful for navigational planning, identifying wave energy resources, providing information for site specific coastal flood models, having an informed recreational beach user group, among other things. This forecasting model is run once a day at 1200 UTC producing 84 hour forecasts. A series of nested grids with increasing resolution shoreward are implemented to achieve a 30 arc-second resolution at the shelf level. This resolution is significantly higher than what the current operational models produce, thus improving the ability to quantify the alongshore variations of wave conditions on the PNW coast. Visualization of the data is made available online and is presently being used by recreational beach users and the scientific community. A series of simulations, taking advantage of having a validated shelf scale numerical wave model, suggest that neither dissipation due to bottom friction or wind generation are important in the region at this scale for wave forecasting and hindcasting. The Astoria and McArthur Canyons; the Stonewall, Perpetua, and Heceta Banks; and Cape Blanco are significant bathymetric features that are shown to be capable of producing alongshore variability of intermediate to shallow water wave heights in this region.

2.1 Introduction

An increasing interest in understanding the ocean waves in the Pacific Northwest (PNW) region of the United States of America has been fueled by an observed multi-decadal increase in wave heights (Allan and Komar, 2000, 2006; Komar et al. 2009; Menéndez et al., 2008; Ruggiero et al., 2010; Seymur, 2011; Young et al., 2011), the potential for harvesting wave energy in the region (Arinaga and Cheung, 2012; Cornett, 2009), and the need to make localized, informed decisions in an evolving climate, such as coastal flood warnings. As waves propagate from deep water to nearshore regions (with water depths of O(20)m), they are affected by the underwater

topography (bathymetry). The US West Coast shelf is characterized by a complex shelf bathymetry with numerous canyons, large banks, capes, and headlands. These features may focus, divert and transform wave energy by the processes of refraction, shoaling, diffraction, and dissipation due to bottom friction and wave breaking. Nearshore wave predictions need to resolve the relevant bathymetric features and account for the associated wave transformation processes.

The National Oceanic and Atmospheric Administration's (NOAA) National Weather Service (NWS) operates a third generation wave forecasting model called WAVEWATCH III®. This model contains the necessary physics to account for nearshore wave transformation processes if the bathymetry at the relevant length scales is defined. However, the current forecasts in the Eastern North Pacific Ocean are produced at a resolution of 15 arc-minutes (19.8km in the cross-shore direction and 27.8km in the alongshore direction at the 44.5°N). At this resolution, there are only 17 computational nodes along Oregon's coast, and bathymetric features along the coast cannot be adequately resolved. Further, due to this coarse resolution, the grid cell that is closest to the shore may be in water depths of as much as 315m, failing to specify the wave field in the nearshore region. Hence, the current forecasting system may not be capable of capturing the alongshore variability of wave conditions necessary for site specific purposes.

To satisfy a range of needs in the PNW a high resolution wave forecasting model was implemented for the Oregon and southwest Washington coast using the WAVEWATCH III version 3.14 numerical model (Tolman, 2002b). This operational forecasting model provides 84 hour forecasts at a 30 arc-second resolution. At this resolution the model provides 510 output points along the Oregon coastline and enables the generation of a high resolution wave climate database. The forecasting system is forced by wind fields and air-sea temperature differences forecasted by NOAA's National Centers for Environmental Prediction (NCEP). In this paper we describe the implementation of the wave forecasting model for the PNW. The operational aspects of the forecast are described, and model validation with available

nearshore wave observations is carried out. We then take advantage of the validated numerical wave model and investigate the dominant wave transformation processes in the region. The importance of including dissipation due to bottom friction and wind generation at the shelf scale is assessed by performing a series of numerical simulations including and neglecting these physical processes. Further, at this high resolution we are able to capture the effect of large scale bathymetric features such as canyons, banks, capes, and headlands. Therefore, we investigate the effect of these features on the nearshore wave field making use of two numerical wave models, WAVEWATCH III v3.14 and Simulating WAves Nearshore (SWAN) numerical model (Booij et al., 1999).

2.2 The US Pacific Northwest

The PNW region of the United States of America, Oregon and Washington, receives hundreds of thousands of visitors yearly that include, but are not limited to, recreational beach users and surfers. For instance, shore-based whale watching gathers more than 126,000 visitors each year in Oregon (Christensen et al., 2007). There are important commercial ports in Astoria and Newport, and in general Oregon experiences high boat traffic activity. The region of interest extends more than 420km from north to south (see Figure 1). The region's shelf is characterized by multiple complex bathymetric features. These include the Astoria, Willapa, Guide, and McArthur Canyons; the Stonewall, Siltcoos, Perpetua, and Heceta Banks; and multiple capes and headlands.

Waves in the PNW vary throughout the year and along the coast. The wave climate in this region is characterized by large wave heights in the winter months. Approximately one event per year exceeds significant wave heights (SWH) of 10m (Ruggiero et al., 2010). The strongest storms recorded in the region have generated offshore SWHs of approximately 15m (Allan and Komar, 2006). Table 1 shows average wave conditions from a record spanning from 1991 to 2009 (inclusive) at

NDBC buoy 46050 (see Figure 1)[1]. This buoy is located 37km offshore in 128m of water. Waves are generally higher in the winter than in the summer. They also tend to be longer in the winter; this indicates that these waves are produced far from the measuring location. Figure 2 shows measured wave data for 2009. During this particular year the maximum wave height reached 9.3m. Further, waves in this region approach from various directions throughout the year, although in general waves tend to come from the northwest during the summer and from the west during the winter.

A multi-decadal increase of significant wave height (SWH) in this region has been well documented during the previous and present decade (Allan and Komar, 2000, 2006; Komar et al., 2009; Menéndez et al., 2008; Ruggiero et al., 2010; Seymour, 2011; Young et al., 2011). Ruggiero et al. (2010) evaluated wave buoy data and reported that the average winter SWH increases annually at a rate of 0.023m/yr. This same report suggests that the rate of increase for the annual maximum SWH is even higher. Gemmrich et al. (2011) found a relatively limited wave height increase and pointed out problems with buoy data prior to 1985. Young et al. (2011) studied the world's wave climate using altimeter data from 1985-2008 and found that the 99th percentile SWH shows a positive trend in the North Eastern Pacific Ocean. Larger waves are a concern because they result in an increase of the dangers associated with ocean related activities. Identifying the reasons and implications of SWH increases is currently the subject of active research, and assessing possible links between increasing nearshore SWHs and changing wind conditions can be aided by the use of a nearshore wave forecasting system for the region. Another purpose of implementing a high resolution wave forecasting model is that alongshore variable wave data will be available in advance to coastal modelers interested in high resolution coastal flood forecasting. During extreme events in the PNW, the wave runup, which is a function of wave height, has been the main contributor to the total water levels along the coast (Allan and Komar, 2002). Hence, localized predictions for flood risk in coastal communities require a high resolution prediction of nearshore wave height.

[1] Oceanographic convention will be used throughout this discussion. Under this convention the direction from which waves are approaching is measured clockwise from true north. Thus, waves

The highly energetic waves off the coasts of Oregon and Washington are also well suited for wave energy harvesting (Arinaga and Cheung, 2012; Cornett, 2009). Many emerging wave energy harvesting technologies are designed to operate in the nearshore ocean in water depths less than 40m (Flacão, 2010). However, most of the long-term observations on this coast are from wave buoys in much deeper water, and there is indication that, at some locations, wave power can be reduced more than 20% when waves approach the nearshore from deep water (Folley and Whittaker, 2009); therefore, a nearshore wave energy characterization is desired. Due to high costs, obtaining long-term wave data in the nearshore at a high spatial resolution along the PNW is not viable. A validated nearshore wave-forecasting system is well suited to provide wave information in these regions. This information can then be used to identify possible sites for wave energy harvesting. Wave forecasts can also inform computations of the near-future energy yield of an installed device for device tuning purposes.

2.3 Numerical Model

The WAVEWATCH III version 3.14 (WW3) (Tolman, 2002b) is the numerical model implemented in this project. This is a third-generation phase-averaged wave model developed by NOAA's National Center for Environmental Prediction (NCEP) that solves the spectral wave action balance equation:

$$\frac{\partial N}{\partial t}+\frac{\partial\left(c_{gx}+U_x\right)N}{\partial x}+\frac{\partial\left(c_{gy}+U_y\right)N}{\partial y}+\frac{\partial c_\theta N}{\partial\theta}+\frac{\partial c_\omega}{\partial\omega}=\frac{1}{\sigma}\left(S_{in}+S_{ds}+S_{nl}+S_{bf}+S_{brk}\right) \quad (1)$$

$$\omega=\sigma+\boldsymbol{k}\cdot\boldsymbol{U} \quad (2)$$

where $N\equiv E/\sigma$ is the wave action for a component and is a function of frequency, direction, time and position; σ is the relative radian frequency; ω is the absolute radian frequency; $\boldsymbol{U}=\left(U_x,U_y\right)$ is the depth- and time-averaged current velocity vector;

$\boldsymbol{k} = (k_x, k_y)$ is the wave number vector with a magnitude k equal to $(2\pi/L)$; and h is the water depth. The left hand side of Equation 1 accounts for the linear propagation of the wave component, the first term represents the local rate of change of wave action, while the next four terms represent the advection of wave action in the x, y, θ, and ω dimensions. The group velocities (c_{gx}, c_{gy}) determine the velocity at which wave action travels in the horizontal plane by:

$$\boldsymbol{c}_g = \frac{\partial \sigma}{\partial k}\frac{\boldsymbol{k}}{k} \tag{3}$$

Energy propagation in the wave number space (c_θ), representing the process of refraction, is given by:

$$c_\theta = -\frac{1}{k}\left(\frac{\partial \theta}{\partial h}\frac{\partial h}{\partial n} + \boldsymbol{k} \cdot \frac{\partial \boldsymbol{U}}{\partial s}\right) \tag{4}$$

where n and s are the coordinates perpendicular to and in the direction of wave propagation, respectively. Energy propagation in the frequency space (c_ω) is represented as:

$$c_\omega = \frac{\partial \sigma}{\partial h}\frac{\partial h}{\partial t} + \boldsymbol{k} \cdot \frac{\partial \boldsymbol{U}}{\partial t} \tag{5}$$

On the right hand side of Equation 1, S_{in} and S_{ds} represent the input and dissipation of energy due to wind and whitecapping, respectively. In this implementation WW3 defaults based on an atmospheric boundary layer formulation are used (Tolman and Chalikov, 1996). S_{nl} are the non-linear quadruplet wave interactions, modeled using the discrete interaction approximation (Hasselmann et al., 1985). S_{bf} is the dissipation by bottom friction represented by the linear JONSWAP formulation (Hasselmann et al., 1973), default value for the bottom friction coefficient $(\Gamma = 0.067 m^2 s^{-3})$ was used. S_{brk} represents dissipation of energy due to depth-induced breaking modeled with the Battjes and Janssen (1978) approach, default values for the wave breaking coefficient $(\gamma = 0.73)$ and intensity of breaking $(\alpha = 1)$ were used. The frequency and wavenumber are related by the dispersion equation:

$$\sigma^2 = gk \tanh(kh) \quad (6)$$

these equations are solved with a third-order explicit propagation scheme (Booij and Holthuijsen, 1987) that includes a scheme to alleviate the Garden Sprinkler Effect (GSE) (Tolman, 2002a). The GSE is a numerical effect that can lead to an unrealistic disintegration of the wave spectrum (Booij and Holthuijsen, 1987). The wave spectrum was discretized in direction with 24 bins spaced at 15° and in frequency with 25 bins using a logarithmic spacing from 0.04118 to 0.5 Hz.

2.3.1 Model Implementation

The present localized forecasting model implementation (hereafter referred to as NearWW3_PNW) is built taking advantage of WAVEWATCH III version 3.14 mosaic nesting capabilities (Tolman, 2006, 2008). In contrast to traditional telescoping nesting, multiple modeling domains interact with each other consolidating data at common time steps. Having multiple nested grids focuses the computational resources where they are needed. Waves in intermediate to shallow waters are affected by the bathymetry; therefore higher resolution is needed as waves approach the shore. In this implementation 4 levels, adding to a total of 6 nested grids, are part of the mosaic. To account for wave generation at oceanic scales we use in-house versions of models based on NCEP's Global and Eastern North Pacific (ENP) grids, making up two levels of nesting. The Global grid provides near-global coverage at a 1.25° by 1.00° resolution, in the latitudinal and longitudinal directions, respectively. It covers a region from the 77°S to the 77°N. With a 15 arc-minute resolution, the ENP covers a region from 5°N to 60.25°N and from 170°W to 77.5°W.

To account for local bathymetric features on the Oregon continental shelf we then assembled a grid (referred to as the "outer" grid) with a three arc-minute resolution in both the latitudinal and longitudinal directions. It covers a region from 41.45°N to 47.50°N and from 127°W to 123.75°W. The shallowest grid cell at the deep water boundary is at 2090m. The outer grid interacts with three highly resolved "shelf" grids that have a resolution of 30 arc-seconds in both the longitudinal and latitudinal

directions. These grid points are spaced 927m apart in the alongshore direction, resulting in 510 cells along the Oregon coast. In the cross-shelf direction the grid spacing varies from 694m to 627m, depending on the latitude. All three shelf grids cover a region from 125.25°W to 123.75°W. The southern grid covers a region from 41.50°N to 43.55°N (see Figure 1). The central one covers a region from 43.40°N to 45.45°N. The northern grid goes from 45.30°N to 47.35°N.

The bathymetry data for the outer and shelf grids were obtained from NOAA's National Geophysical Data Center (NGDC). In 2006 the NGDC started building high resolution digital elevation models (DEM) at the US coast (Carignan et al., 2009a,b,c,d; Grothe et al., 2011, 2010). This data set was chosen because these DEMs carefully incorporate many available public surveys, coastline databases and lidar surveys. Their resolution at the US west coast is one-third of an arc-second. The western boundary of these DEMs does not always extend to deep water; therefore, they were combined with ETOPO1 gridded bathymetry (Amante and Eakins, 2009).

Finally, the implementation of a wave forecasting model requires atmospheric data in order to force the model. The nearshore operational forecasting model developed herein is driven by wind fields at 10m elevation above the water surface produced by the Global Forecasting System (GFS) as atmospheric input (Sela, 1980; Environmental Modeling Center, 2003). The GFS is executed four times a day (00, 06, 12, 18 UTC) by the NCEP. The current model version 9.1.0 has a horizontal resolution of roughly half a degree in both the latitudinal and longitudinal directions. To account for boundary layer stratification, air and sea temperatures are obtained from NCEP's Global Data Assimilation System (GDAS). The air-sea temperature difference is computed and, along with the wind fields, are used to determine the wave growth with the Tolman and Chalikov (1996) source terms. The wind fields that force the wave model act on all grids, linear interpolation in time and space are used to apply them at every time step and grid cell. At this moment, NearWW3_PNW neglects ocean and wave-driven currents.

2.3.2 Operational Wave Forecasting

NearWW3_PNW has been operational since May 2011. At the time of this writing, the model is executed twice a day. The first model run is aimed at updating the initial conditions for the forecasting model. This first run is initiated at 1300 UTC on any given day and involves an 18 hour hindcast for the conditions between TAU -24 and TAU -6. Note that wave hindcasting is the prediction of waves based upon past analyzed meteorological and oceanographic data (Rao and Mandal, 2005), so the hindcast involves higher quality input and forcing data. The model run then continues with a short range 6 hour forecast until TAU 00, resulting in an estimate of the conditions at 1200 UTC on the current day. For this run, GDAS analyzed, 3 and 6 hour forecasted winds, and air-sea temperature differences from the last four NOAA runs are used to force the model. This model run, therefore, performs a 24 hour computation with higher quality input and forcing.

Starting from the estimated conditions for 1200 UTC, we then perform a wave forecast with a TAU +84 hour horizon. For the wave forecasting model, wind forecasts are downloaded from the GFS ftp server at 1610 UTC, and the forecasting model is initiated immediately. Currently, the model runs on 44 threads on two UNIX servers that have two six core Intel Xeon CPUs clocking at 2.7 GHz. The forecasts are completed around 0100 UTC of the next day, and forecasts for nearly 3 days (~71 hours) become available at that time. Spectral output is being produced at buoys 46211, 46243, 46029, 46050, 46229, and 46027 (see Figure 1) as well as at a site in 40m of water depth near Reedsport, Oregon. Bulk wave parameters are stored at every grid cell and are made available upon request in WMO's GRIB1 format.

2.3.3 Wave Hindcasting

NearWW3_PNW can also be executed in hindcast mode. These hindcasts are performed to validate the model with shallow water *in situ* measurements that were gathered in the past. Wind forcing for these simulations comes from the NOAA NCEP GFS reanalysis; in other words these are analyzed wind fields instead of forecasted, therefore resulting in higher quality input. Consequently, hindcast performance most

closely characterizes errors in the wave model physics; forecast errors could be higher than these because of compounding errors associated with the wind forecasts. To validate NearWW3_PNW, three hindcasts were performed; during the Autumn 2009, Summer 2005 and Autumn 1999. These times were selected based on the availability of ground truth data as explained in Section 2.4.1.

2.4 Model Accuracy

In order to validate this implementation, model data is compared against *in situ* data. To quantify the performance of NearWW3_PNW, root-mean-squared error (RMSE), normalized root-mean-squared error (NRMSE), bias, and linear correlation coefficient (r2) will be used throughout the discussion. Details regarding the definition of these metrics are described in the Appendix.

2.4.1 Data Sources

We compared model results with available *in situ* wave data within the region covered by our high resolution domains. We had access to shallow water wave data collected during three field experiments. These are described in Table 2 and experiment locations are shown in Figure 1. Both the RP09 and NP05 deployments used Acoustic Wave and Current Sensors (AWAC) to measure wave activity. These sensors track the water surface and particle velocity, and these data was converted to wave spectral information by making use of linear wave theory. The RP09 deployment covered a period from 18 September 2009 to 2 December 2009. During this deployment the average SWH, peak wave period (PWP, calculated from the frequency spectrum using a parabolic fit around the discrete peak), and peak wave direction (PWD, calculated from the direction spectrum in the same fashion as PWP) where 2.5m, 11.1s, and 291°, respectively. The maximum recorded SWH during this experiment was 6.8m while the longest recorded PWP was 19.9s.

The NP05 data consists of an initial deployment (NP05S) near Newport, Oregon at 15m water depth from 15 June 2005 to 13 July 2005 (for a complete description of the data collection from this experiment the reader is referred to Kirincich et al. (2009).

During the deployment time the instrument recorded average SWH, PWP, and PWD of 1.3m, 8.5s, and 284°, respectively. The maximum recorded SWH was 4.0m. A second deployment (NP05N) took place north of the first one at 13m water depth from 23 July 2005 to 22 September 2005. During the deployment time the instrument recorded average SWH, PWP, and PWD of 1.3m, 8.9s, and 281°, respectively. The maximum recorded SWH was 3.4m.

The GH99 data was collected as part of the Grays Harbor Wave Refraction Experiment of 1999 (Gelfenbaum et al., 2000). Wave information was collected using a pressure sensor. These sensors record pressure fluctuations and making use of linear wave theory wave spectral data may be acquired. We considered data from two stations from this experiment, ND and SD[2]. ND was located northwest of Ocean Shores, Washington and deployed twice, from 1 October 1999 to 2 November 1999 at 23m water depth and from 5 November 1999 to 29 December 1999 at 25m water depth. The SD station was located south of ND near Westport, Washington. It was also deployed twice at 22m water depth from 2 October 1999 to 27 November 1999 and from 27 November 1999 to 29 December 1999. During the deployment time ND registered average SWH and mean wave period (MWP) of 3.3m and 11.3s, respectively[3]. Throughout, this discussion MWP will be used to refer to $T_{m01}(= 2\pi m_0/m_1)$ where $m_n = \int \omega^n \zeta(\omega) d\omega$ and $\zeta(\omega)$ is the variance frequency spectrum. This experiment was performed during a very energetic time, with four events exceeding SWH of 7m and a maximum event of 9.7m.

Since the model provides shelf scale coverage, data from buoys located in the region were considered. These are long term deployments maintained by NOAA's National Data Buoy Center (NDBC) or the Coastal Data Information Program (CDIP) from the Scripps Institution of Oceanography in La Jolla, California. Table 3 shows details on the nature and location of these buoys, which are mapped in Figure 1. These buoys undergo periodic maintenance and are sometimes damaged and go out of

[2] In this article we use the same nomenclature that was used to refer to these locations in Gelfenbaum et al. (2000).
[3] Only significant wave height and mean wave period data was distributed.

operation during severe weather conditions, therefore the data is not always continuous. For this study only quality controlled data were used to evaluate the performance of the model (for more information on the quality controls performed by NDBC the reader is referred to NDBC (2009)).

2.4.2 Hindcast and Forecast Performance

In order to assess hindcast performance, a total of three simulations were carried out. These cover the period of available shallow water wave data and analyzed wind fields. Two hindcasts covered roughly three months each, one from September to November 2009 and the other from mid-June to mid-September 2005; and a third hindcast covered the months of November and December 1999 (see Table 2). Model agreement with available buoy data during these same hindcast periods was also evaluated. The performance statistics are summarized in Table 4. For all the performed hindcasts, the predicted SWH is highly correlated with observations ($r2>0.83$); this is consistent with existing high-resolution localized wave forecasting systems (Alvarez-Ellacuria et al., 2010). For Autumn 2009 and Summer 2005, RMSE's range from 0.20m to 0.57m resulting in percent errors in wave height (NRMSE) of 13-23%. The largest errors in the SWH predictions occur for the 1999 hindcast (up to 0.88m, or 24%, errors), and this may be due to the difference in quality of the wind fields. The GFS model has been updated numerous times over the last decade; including resolution increases and additional physics, among other things, and the analyzed winds for 1999 are likely less accurate than those for 2005 and 2009. Nevertheless, even with inferior wind forcing the model still shows a good agreement, resulting in high correlation coefficients. Biases are smaller for the Autumn 2009 hindcast, and large negative biases (indicating underprediction) are present for the 1999 hindcast. The MWP is predicted with ~1.5s error for the 2009 and 2005 data sets. Errors for the 1999 data sets are about twice as large, with the bias indicating underprediction. Correlation values for the MWP are not as high as those associated with the SWH predictions.

Forecast accuracy can be characterized by comparing the forecasts at different TAUs with the actual measured conditions. Figure 3 shows NRMSE in SWH as a

function of forecast hour for the six NDBC or CDIP buoys in our region of interest from October to December 2011 when the average SWH, PWP and PWD at buoy 46050 were 2.9m, 12.0s, and 282°, respectively. As expected, forecast accuracy is similar to the hindcast accuracy at time 0 (~17-19%), but then declines slightly with forecast hour. This decline is a function of the forcing uncertainty since the wind forecast error increases with forecast time as well. However, the forecast accuracy decreases only by about 10 percentage points (to 19-22%) over 72 hours. Hence, NearWW3_PNW produces accurate forecasts even at the 72 hour horizon.

2.4.3 Seasonal Performance

To assess the possibility of a seasonal trend in model performance, a four year hindcast was performed including the Global, Eastern North Pacific and outer domains from 2007 to 2010. The SWH prediction was evaluated by monthly averaging the NRMSE and bias metrics for the deeper water buoys 46229, 46050 and 46029. Since these buoys are located in relatively deep water, the shelf grids were not included in the hindcast. Results are plotted in Figure 4 for these three buoys; discontinuities are due to the absence of measured data. The bias metric indicates that the SWH is often overpredicted. The bias shows larger errors during the winter months similar to what Hanson et al. (2009) saw. However, this is also when wave heights are larger. Consequently, the NRMSE metric does not show an appreciable seasonal trend. The errors are uncorrelated among these buoys, therefore we conclude that no seasonal trend affects this model implementation.

2.4.4 Comparison with Existing Operational Model

NearWW3_PNW provides over 600 points along the Oregon and Washington coast, capturing the distinctive alongshore bathymetric features of the region and taking them into account for the wave forecasts. The left panel of Figure 5 shows the SWH interpolated to the 250m contour along the modeling domain for both NearWW3_PNW and the NCEP ENP model. Discontinuities in the lines exist because at 42.75°N the shallowest grid point of the ENP model is at 315m water depth. The

higher resolution allows for the representation of features such as the Astoria Canyon. Canyons divert wave energy by the process of refraction, thus reducing the wave energy density. This is shown as a reduction in the wave height near the 46.25°N, the effect of the canyon in the nearshore wave field is discussed in Section 2.5.2.2. The central panel of Figure 5 shows the amount of information provided at the 20m contour by both operational models. NearWW3_PNW provides near complete coverage of this region. At 20m water depth, the current implementation has 99% active cells while the ENP model has 4% (see Figure 6). This metric is based on all potential wet cells outside of the land contour for each model latitude as a function of water depth. If the cell is on water depths deeper than the one evaluated, it is considered dry. This is important for runup analysis because modern formulations are based on local SWH at approximately 20m water depth (see for example Stockdon et al., 2006).

As previously mentioned, many emerging wave energy devices are intended to be deployed in shallow water. To estimate expected power output, wave forecasts are needed where the wave energy device is located. Figure 7 shows forecasted SWH along 42.75°N by the NCEP ENP model and NearWW3_PNW. The current operational model is incapable of resolving the wave field in the nearshore and does not provide any data in some regions. NearWW3_PNW provides data up to the 20m contour capturing the wave transformations due to the topography at the shelf scale. Thus both implementations are complementary, one providing open ocean forecasts and NearWW3_PNW providing shelf scale coverage.

2.5 Dominant Wave Transformation Processes

Taking advantage of the assembled and validated wave forecasting model along the entire Oregon and the southwest Washington coast, we investigate effects of isolated physical processes in the region. First, we will analyze the importance of bottom friction and wind input over the continental shelf. For this purpose *in situ* shallow water ground truth data was compared to a series of simulations where these physics were omitted. Further, we investigate the effects of refraction over bathymetric

features on the continental shelf by studying test cases in which the nearshore wave field may be altered by offshore features. For these the NearWW3_PNW hindcasts were complemented with a different numerical model, SWAN (see Section 2.5.2).

2.5.1 Effect of Bottom Friction Dissipation and Wind Input

The PNW region is characterized by a relatively narrow continental shelf, with length scales in the order of ~15 to ~60km (0.2°-0.8°). This raises the question of the relative importance of including bottom friction and wind forcing at the shelf scale. To evaluate this, a series of one-way nested hindcasts were performed for the RP09 and NP05 data (see Section 2.4.2). One-way nesting was selected in order to completely isolate the shelf level grids from those that produced the boundary conditions. Alongshore varying boundary conditions were generated by the three lower-resolution models (Global, ENP, and outer). These low-resolution hindcasts include all the physics used for the validation runs and the operational forecasts with the exception of stability correction for wind growth as described by Tolman (2002b). Exclusion of this correction translates into smaller wave heights, which becomes evident when comparing these results with the validation data.

SWH was computed from the different hindcasts at the location of the *in* situ data and the time series were compared by computing the performance metrics described in the Appendix; the results are summarized in Table 5. In general, there are no appreciable differences when comparing the time series generated by each model execution. The model performance is not significantly affected regardless of the considered physics, suggesting that neither bottom friction or wind growth are important at the shelf scale for wave modeling in the PNW and likely in locations with similar shelf characteristics. Only the bias metric is slightly affected, both cases that exclude wind wave generation show a larger negative bias than those that include it. The simulations that excluded the winds also excluded whitecapping, the process is responsible for steepness-limited wave breaking dissipation. An additional simulation was performed that neglected wind input but included whitecapping dissipation for the NP05S station. Wave heights at this station show a larger negative bias than the other

cases, meaning that whitecapping is responsible for the observed reduction in the wave energy. Thus, whitecapping has a bigger impact than wind generation in these locations. Nevertheless, the differences are on the order of 5cm, therefore we conclude that neither dissipation due to bottom friction or wind generation are important for wave forecasting/hindcasting at the shelf scale in this region. It is worth mentioning that our analysis does not include the surf zone, where depth-limited wave breaking is expected to be the dominant dissipation mechanism.

2.5.2 Effect of Wave Refraction over Bathymetric Features

In this section we investigate the effect of large scale bathymetric features on the shallow water wave field in the PNW. From the hindcasts described in Section 2.4.2 we identified three interesting sets of features, they are: the Stonewall, Heceta and Perpetua Banks; the Astoria and Willapa Canyons; and Cape Arago and Cape Blanco. In the following subsections we will evaluate wave transformation processes near these features. First we will identify cases where wave modifications due to the features of interest are evident.

Our simulations show that the banks have the ability to focus energy in certain locations shoreward. During the autumn of 2009 there were several events where waves had peak periods in the excess of 10s. For example, 7 November 2009 conditions (shown in Figure 8) indicate the possibility of wave focusing shoreward of the Stonewall Bank (right panel). Wave height is focused at certain locations offshore Newport and Waldport. However, when examining the wave field at the 20m contour (left panel), there is no clear evidence of variations at the scales of the wave focusing. The wave height at the 20m isobath responds to shallower bathymetric effects with smaller length scales. Hence we investigate under which, if any, conditions the waves at the 20m contour can contain alongshore variability at length scales related to the banks. Being interested in large scale behavior in this discussion, we introduced a running average to smooth the SWH plots on a contour; its effect is shown in Figure 8 to Figure 10 and Figure 12. The large scale variations are preserved by the smoothing while the small scale signals are eliminated. This averaging replaces all SWH values

with the average value of a specified stencil, in the remaining graphs where we plot SWH at a contour, the stencil width varies from 11 to 15 points with the replaced value in the center.

In our northern domain, the bathymetry is radically different. Instead of being dominated by banks it is dominated by canyons. Contrary to banks, these divert wave energy. When evaluating our hindcasts, strong alongshore gradients in wave height were identified at the 20m isobath in the northern coast of Oregon and the southwest coast of Washington. Figure 9 shows results from the Autumn 2009 Hindcast at this location for the 7 November 2009 conditions when long waves approached from the northwest. Several focusing and defocusing regions are evident and are associated with the canyons, especially the Astoria and Willapa canyons.

In southern Oregon, the shoreline shows a change in orientation near Cape Blanco. Results from the Autumn 2009 Hindcast near Reedsport, OR, indicate lower wave height regions to the north of Cape Blanco and Cape Arago when waves approached at angles less than 225° (from the southwest). Figure 10 shows the results for 2300 UTC 5 November 2009 when this effect is evident.

All example cases discussed above show a decrease in the wave height shoreward of the 150m contour, even in areas with nearly straight-and-parallel contours. Several potential processes can give rise to such a decrease. Bottom friction or other dissipational processes may be at play; however, analysis in the previous section showed that these processes affect the predicted wave height minimally on this shelf. Refraction of obliquely incident waves (even over straight-and-parallel contours) is another process that would cause a sustained decrease in the wave height with decreasing water depth since the wave energy is distributed over a longer wave crest as the wave refracts towards shore (see Dean and Dalrymple, (1991)). Finally, the group velocity of waves shows a small increase as waves first start feeling the presence of the bottom before the steady decrease as water depth decreases further. Conservation of energy flux dictates that the wave shoaling process will then result in a decrease in wave height before a sustained increase in wave height with decreasing

depth. This behavior is predicted by linear wave theory and has been observed in the laboratory (Iversen, 1952).

All cases also show alongshore variability in wave conditions that appear to be linked to the identified banks, canyons and capes. However, temporal and spatial variability associated with arriving storms can also induce alongshore variability in the nearshore even in the absence of any bathymetric features. In order to isolate the effect of wave transformation over bathymetry while eliminating possible effects related to variability of the offshore wave field, we perform a series of idealized simulations using the wave transformation model SWAN which allows for alongshore-uniform conditions at the offshore boundary and the determination of a steady-state solution.

The third-generation phase-averaged spectral wave model SWAN is a well-established wave propagation and transformation model that, similar to WAVEWATCH III v3.14, solves the action balance equation. In this study we use version 40.81. SWAN has been proven skillful in simulating waves over the complex US west coast bathymetry (Gorrell et al., 2011; Rogers et al., 2007). By implementing this model in our domain, a careful evaluation of the effects of the aforementioned features can be accomplished. Simulations with this model were performed on the same shelf grids as those used in NearWW3_PNW. Whenever SWAN simulations were used, the model was run in steady state mode ($\partial N/\partial t = 0$ in Equation 1) and no source or sink terms other than depth-limited wave breaking dissipation were considered (e.g. wind input, whitecapping dissipation, quadruplets, bottom friction). Wave breaking was estimated with the Battjes and Janssen (1978) approach with the default wave breaking coefficient (γ=0.73); same parameterization used in the WAVEWATCH implementation. The model was forced with alongshore-uniform conditions at the offshore boundary. The lateral boundaries (i.e. north and south) were extended 50 arc-minutes (~92km) to the north and to the south assuming straight and parallel contours and a one-dimensional model run was executed at the top and bottom latitude. As opposed to WAVEWATCH, which uses an explicit propagation scheme, it solves Equation 1 with an implicit second-order numerical scheme; this

implementation uses the default for stationary computations (more details in Rogers et al. (2002)). SWAN was executed in spherical coordinates over the same NearWW3_PNW shelf grids. 24 logarithmically spaced frequency bins from 0.04118 to 0.50 Hz were considered and the directional resolution was 5°. With this additional tool we investigate the conditions that lead to variability in the nearshore waves (at the 20m contour) and also identify the responsible wave transformation process.

2.5.2.1 Stonewall, Heceta and Perpetua Banks

In this section we will investigate under which conditions the Stonewall, Perpetua and Heceta banks affect the wave field at the 20m isobath. The Stonewall Bank, located near Newport, OR, reaches depths as shallow as 50m at more than 20km offshore. Southwest of the Stonewall Bank are the Perpetua and Heceta Banks, both with water depths as shallow as 80m. According to linear wave theory, waves with periods larger than 10s may be affected by these features. Two questions were of particular interest to us, determining which physical process is responsible for the predicted wave transformation, and documenting under which conditions the banks affect the nearshore waves.

To separate the effects of shoaling and refraction, three SWAN simulations were carried out including both two-dimensional refraction processes and shoaling (hence, the full model) in Case A, only shoaling in Case B, and shoaling along with a one-dimensional refraction[4] formulation assuming straight-and-parallel contours at the selected transect in Case C (see Figure 11). Note that differences between Cases B and C identify modifications due to refraction that would occur even if focusing around the banks was not present. Differences between Cases A and C highlight the focusing effects of the banks. All simulations are forced by a 2D JONSWAP spectrum on all open boundaries. The spectrum used for each simulation was based on the hindcasted wave spectrum at Buoy 46050 for 1200 UTC 7 November 2009 (corresponding to the case in Figure 8). At this time the hindcasted spectral parameters were SWH of 7.6m,

[4] This is in essence similar to performing a 1D SWAN simulation, however as of version 40.81 this model does not have the capability of performing such computations on a spherical grid.

MWP of 16.3s, and PWD of 293°. This is a rather large wave height; however, SWAN is essentially a linear wave propagation model, hence results outside the surf zone are not sensitive to the absolute value of wave height.

The top panel in Figure 11 shows transects of wave height at 44.5°N for the three aforementioned SWAN simulations. All three cases display the wave height decay entering intermediate water depths (124.7°W), indicating that the decay is due to the shoaling process associated with the localized increase in the group velocity. The wave power ($PWR=Ec_g$) is not altered in the absence of refraction, therefore group velocity has to increase correspondingly (see 3rd panel). Case A, which includes refraction on alongshore varying bathymetry, shows increased wave height shoreward of the bank. This is the region of wave focusing due to refraction on the banks, since shoaling is not the dominant process the wave power increases in these locations. In the focusing region, an increase in the directional spreading (DSPR), which is defined as the standard deviation of the direction spectrum, is expected because waves turn around the shoal into the focusing zone (see 2nd panel in Figure 11). Cases B and C, which do not include two dimensional refraction, exhibit minor wave recovery shoreward of the bank due to deshoaling. Note that Cases A and B predict a similar wave height just shoreward of 124.2°W, indicating that the effects of wave focusing are no longer apparent shoreward of this location.

To understand under which conditions the waves are amplified at the 20m isobath, a series of simulations were performed with the same JONSWAP spectrum as before for multiple directions (ranging from 240° to 300°) and periods (ranging from 8s to 20s). These series of simulations as well as those in the following sections will use the same JONSWAP peak enhancement parameter with a value of 3.3 and a directional spread of 20°. Example results for 250° wave incidence (corresponding to waves from the southwest) and 16.3s waves (see Figure 12) indicate a wave focusing area offshore of Newport, OR, between 44.2°N and 44.6°N. Figure 13 shows a series of wave heights at 20m water depth for different angles of incidence. When waves approach from the southwest (left panel) the wave focusing becomes evident between 44.2°N

and 44.6°N. The position of this amplified zone is a function of the incidence angle; as waves approach more perpendicular to shore, the zone is displaced southward. When waves approach from the northwest, this amplified zone moves further south losing its intensity. This is related to the enhanced focusing effect when waves approach from the southwest (compare Figure 12 and Figure 8) causing a larger focusing region that is still effective at the 20m contour. In contrast, the focusing region for northwesterly wave incidence is wider but does not extend as far towards the shore. The magnitude of this amplification is correlated with the wave period (see Figure 14). The longer wave periods produce greater alongshore variability for the same SWH and PWD. Hence, wave amplification in this zone is strongest for long waves coming from the southwest direction.

2.5.2.2 Astoria and Willapa Canyons

The Astoria Canyon is one of the most distinct features on the PNW shelf. The canyon's head is approximately 18km west of the Mouth of the Columbia River (MCR) with an approximate water depth of 100m (Astoria Canyon, 2012). Further north, the Willapa Canyon heads at approximately 35km west of Ocean Park, Washington. In contrast to banks, canyons divert wave energy but by the same physical process, refraction. Our interest is to determine whether the wave field at the 20m isobath along the northern Oregon and southwest Washington coast show large scale variations due to the presence of the canyon. A series of SWAN simulations were performed based on the hindcasted conditions on 1200 UTC 7 November 2009 at Buoy 46029 forced by a JONSWAP spectrum uniformly along the offshore boundary with SWH of 8m; with multiple periods and directions.

Figure 15 shows a series of SWH plots at the 20m isobath as a function of wave incident angle for 8s waves. When waves approach from the southwest (left panel), wave energy is diverted and a shadow zone appears in the southern part of the Long Beach Peninsula (labeled as LBP). This shadow zone lies south of an area where wave energy is concentrated. This energy concentration occurs because both the Willapa and Astoria Canyons divert wave energy. In the area between them, the diverted wave

energy is concentrated. Similar patterns were also predicted for the Scripps and La Jolla Canyons in CA (see, for example, Long and Özkan-Haller (2005)). This creates significant gradients in alongshore SWH; for example when waves approach at 240° the normalized wave height increases from 0.79 at 46.38°N to 1.05 at 46.51°N; this corresponds to a 25% difference in a distance of only 14km. These gradients are produced by the presence of the canyons; otherwise Long Beach Peninsula has almost straight-and-parallel contours where this behavior would not be expected to occur.

The Willapa Canyon shelters the Long Beach Peninsula when waves approach from the northwest (central panel in Figure 15), although to a lesser extent than the sheltering provided to this same area by the Astoria Canyon when waves approach from the southwest (left panel in Figure 15). When waves approach from the northwest, the Astoria canyon diverts wave energy and shelters the Clatsop Plains (also see Figure 9). Not only does the canyon reduce the waves in this region, but the nearshore bathymetry also contributes since the isobaths (see right panel Figure 15) are concave shaped. As an example, when waves approach at 300°, their average offshore normalized wave height is 0.64 near the tip of the canyon at 46.20°N but exceeds 0.95 22.2km south at 46.00°N. For wave incidence from the southwest, sharper wave height gradients exist on the northern side of the shadow regions than on the southern side. This is consistently the case for all the canyon shadows in the domain.

Figure 16 shows results from 7 simulations with waves approaching at 300°. As expected, longer period waves are affected to a larger extent producing larger alongshore gradients at the 20m isobath. For example, the wave height difference between 46.20°N and 46.28°N (a distance of 8.9km) is more than twice as large for 20s waves compared to the case involving 8s waves. Nonetheless, even waves as short as 8s still attain significant alongshore variability in the Clatsop Plains. Since at this wave period the effect of the canyons is rather small, these are present due to the local concave shaped contours as suggested above. Therefore, it is expected that this zone experiences smaller waves that neighboring locations for a wide array of wave

conditions. Further sheltering is present for longer waves because these experience refraction on the Astoria Canyon in addition to the local one, both reducing the wave density.

2.5.2.3 Cape Blanco

Cape Blanco, located 10 kilometers north of Port Orford, OR is easily distinguishable as the westernmost location of the state. The orientation of the coastline changes significantly at this location, and the coastline to the north of Cape Blanco faces towards the northwest by approximately 15 arc-degrees (see Figure 17). Cape Arago is another location where the shoreline orientation adjusts, and the beach to the north of Cape Arago faces further northwest. The bathymetry contours indicate two subtle large-scale embayments in this region, one between Cape Blanco and Cape Arago and one north of Cape Arago. Such embayments are expected to cause refraction patterns that divert the energy away from the middle of the embayment and focus energy near the edges (Long and Özkan-Haller, 2005).

A series of SWAN simulations were performed in this region for varying wave incidence angles, Figure 17 shows SWH plotted at the 20m isobath as a function of MWD. Results indicate that highly obliquely incident waves from the south are affected by the presence of the capes and the associated bathymetric features. The effect is more pronounced for a more oblique the angle of incidence. For example, at 42.95°N waves are more than 30% smaller for MWD of 220° than for 270°. At these high incidence angles, the wave direction is almost parallel to the bathymetric contours just offshore of Cape Blanco and also of Cape Arago (see Figure 10), hence strong refraction has to occur. The reduced wave heights are a result of this process, although simulations neglecting refraction show that the shoaling mechanism identified as responsible for the gently decline of the wave height on the shelf also plays a minor role here. The wave height patterns in Figure 17 indicate a consistent picture. The wave height is severely reduced immediately to the north of each cape creating a large local alongshore gradient in wave height. A milder wave height increase then follows. The resulting pattern can be interpreted as wave sheltering due

to the presence of the capes, similar to the sheltering caused by refraction around the banks or canyons.

Figure 18 shows SWH at the 20m isobath as a function of wave period for a wave incidence of 220°. We find that the effect is relatively insensitive to wave period. This is because the bathymetric features associated with the capes are in very shallow water where even relatively short waves are affected by them. Nonetheless, for PWP of 8s the effect is somewhat reduced.

2.6 Conclusions

In this paper, we describe and assess the performance and implementation of a high resolution wave forecasting model for the Oregon and southwest Washington coast. The performance assessment indicates an improvement in our ability to forecast nearshore wave conditions in comparison with existing operational forecasting models. This model excels in capturing the alongshore variability of the wave field when compared to current operational models by resolving the major bathymetric features on the continental shelf. WAVEWATCH III version 3.14 proved to be skillful in intermediate to shallow waters in the PNW. This model tends to overpredict the SWH and shows no seasonal fluctuations when normalizing the significant wave height error. Having a dedicated wave forecasting system at this coast provides the flexibility to output wave data where stakeholders, recreational users and people interested in wave energy need it. The forecasts are available online at no cost to the user via the NANOOS NVS interface (Risien et al., 2009). At the moment of this writing we are providing spatial plots of SWH, PWD and PWP for each forecast hour in addition to spectral and bulk parameter data at 233 locations with a 2km resolution along our domain at the 25m contour.

The Stonewall, Perpetua, and Heceta Banks; the Astoria and McArthur Canyons; and Capes Blanco and Arago are significant bathymetric features that are shown to be capable of producing significant alongshore variability of shallow water wave height in this region. For the bank systems, we find a wave amplification zone near Newport, OR, for waves approaching from the southwest. The amplification zone occurs further

south for more normal wave incidence and disappears for waves from the northwest. For the canyons systems, we find several focusing and defocusing areas. Their locations are highly sensitive to the wave incidence angle, although they exist for waves from any incidence angle. Locally large wave height gradients are generated near the edges of the sheltering zones. Finally, we find that Cape Blanco and Cape Arago are associated with a change in orientation of bathymetric contours. This gives rise to locally large incidence angles and induces severe wave refraction, resulting in a sheltering zone to the north of the canyons for large incidence angles from the southwest. Note that such highly oblique waves from the southwest are not uncommon (see Figure 2) but waves do not tend to approach at similar incidence angles from the northwest.

The magnitude of the effects for the banks, canyons and capes is a function of the wave period, though more so for the bank systems where the focusing effect is no longer discernible for waves with periods less than 10s. In contrast, for the canyons and capes the sheltering or focusing effects are still evident even for waves as short as 8s, albeit with a reduced magnitude. This is related to the shallower area of influence of the canyons (that protrude shoreward to the 100m contour) and the capes (that are most effective at the shallowest depths).

We note that the wave height in nearshore waters along the 20m contour was consistently less energetic compared to the offshore wave field. We find that this is not related to wave dissipation processes (such as bottom friction, or whitecapping) but, rather, it is controlled by wave shoaling on the continental shelf. In the water depths considered in this study depth-limited wave breaking does not play a significant role in the wave dissipation. Wave shoaling processes cause a reduction in the wave height from the outer edge of the continental shelf to the inner shelf. This is related to the associated slight increase in the group velocity of the waves predicted by linear wave kinematics.

Acknowledgements

We wish to thank the Northwest Association of Networked Ocean Observing Systems for their contributions in the data dissemination. We also thank the investigators who obtained the observations used for the data-model comparisons. In particular Jack Barth, Anthony Kirincich, Ata Suanda, and their field crew obtained to RP09 and NP05 data sets. The RP09 data collection was funded by the Oregon Wave Energy Trust (OWET), the NP05 was gathered through the Partnership for Interdisciplinary Studies of Coastal Oceans (PISCO), funded primarily by the Gordon and Betty Moore Foundation and David and Lucile Packard Foundation. We thank the U.S. Department of the Interior's United States Geological Survey and the Washington State Department of Ecology for providing the GH99 data. Also, we thank the NOAA's National Weather Service for providing the WAVEWATCH III source code and colleagues Sarah Kassem and Gregory Wilson for helpful discussions.

The work presented in this paper was supported by Oregon Sea Grant under Award Number NA10OAR4170059 and by the United States Department of Energy under Award Number DE-FG36-08GO18179. Neither the United States Government nor any agency thereof, nor any of their employees, makes any warranty, expressed or implied, or assumes any legal liability or responsibility for the accuracy, completeness, or usefulness of any information, apparatus, produce, or process disclosed, or represents that its use would not infringe upon privately owned rights. Reference herein to any specific commercial product, process, or service by trade name, trademark, manufacturer, or otherwise does not necessarily constitute or imply its endorsement, recommendation, or favoring by the United States Government or any agency thereof. The views and opinions of the authors expressed herein do not necessarily state or reflect those of the United States Government or any agency thereof.

Table 1: Average wave statistics at buoy 46050 recorded from 1991 to 2009. Winter is considered from October through March. SWH, PWP and PWD stand for significant wave height, peak wave period, and peak wave direction, respectively.

Time Period	SWH m	PWP s	PWD deg
Annual	2.4	10.8	282
Winter	3.0	12.2	273
Summer	1.8	9.5	289

Table 2: Short term wave data sources. ADP stands for Acoustic Doppler Profiler.

Identifier	Depth	Operation	Location	System
RP09	40m	Autumn 2009	Offshore Reedsport, OR	Acoustic Wave and Current Sensor
NP05	13-15m	Summer 2005	Offshore Newport, OR	Acoustic Wave and Current Sensor
GH99	22-25m	Autumn 1999	Offshore Grays Harbor, WA	ADP and pressure sensor

Table 3: Long term wave data sources.

Identifier	Depth	Operation	Location	System
Buoy 46029	135m	Since 1984	37km west of Columbia River Mouth at Oregon and Washington Border	3-meter Discus
Buoy 46050	128m	Since 1991	37km west of Newport, OR	3-meter Discus
Buoy 46229	187m	Since 2005	Offshore Umpqua, OR	Waverider
Buoy 46211	38m	Since 2004	Offshore Grays Harbor, WA	Waverider
Buoy 46243	25m	Since 2009	Clatsop Spit, OR	Waverider
Buoy 46027	48m	Since 1983	15km west-northwest of Crescent City, CA	3-meter Discus

Table 4: NearWW3_PNW Validation Table. N is the number of observations, RMSE is the root-mean-squared error in meters, NRMSE is the normalized root-mean-squared error, and r2 is the linear correlation coefficient. For the 1999 and 2005 hindcasts, only the high-resolution shelf grid that included the short term deplyment was used. All three high-resolution shelf grids were used in the Autumn 2009 hindcast. Mean wave period data was not available for th RP09 and buoy 26229 durimg the Summer 2005 hindcast.

				Significant Wave Height				Mean Wave Period			
Hindcasted Period	Buoy	N	Depth	RMSE	NRMSE	Bias	r2	RMSE	NRMSE	Bias	r2
			m	m	-	m	-	s	-	s	-
Autumn 2009	RP09	1729	40	0.49	0.20	0.19	0.93	-	-	-	-
	46229	2555	189	0.48	0.19	0.08	0.93	1.16	0.18	0.77	0.87
	46050	2511	123	0.50	0.19	0.11	0.93	1.45	0.23	1.17	0.84
	46243	661	25	0.57	0.17	-0.01	0.91	1.28	0.23	0.64	0.78
	46029	2561	135	0.50	0.17	0.06	0.94	1.44	0.24	1.14	0.83
	46211	2496	38	0.49	0.20	0.06	0.92	1.18	0.19	0.69	0.81
	46027	2465	48	0.55	0.23	0.02	0.85	1.55	0.23	1.30	0.84
Summer 2005	NP05N	1477	13	0.20	0.13	-0.06	0.92	1.25	0.22	1.08	0.87
	NP05S	666	15	0.27	0.16	-0.02	0.83	1.44	0.26	1.28	0.66
	46229	2280	189	0.45	0.20	-0.29	0.87	-	-	-	-
	46050	2593	123	0.40	0.19	-0.25	0.88	1.44	0.26	1.14	0.70
November 1999	ND	1310	25	0.88	0.20	-0.54	0.86	3.40	0.24	-2.31	0.57
	SD	751	22	0.85	0.20	-0.50	0.88	3.53	0.24	-2.33	0.53
October 1999	ND	722	23	0.65	0.24	-0.38	0.92	2.37	0.20	-1.31	0.59
	SD	1127	22	0.76	0.22	-0.38	0.88	2.41	0.26	-1.13	0.47

Table 5: Friction and Wind Input Effect. Inclusion of physical process in the modl run is marked by an "X". Root-mean-squared errors (RMSE), normalized root-mean-squared error (NRMSE), bias, and linear correlation coefficient (r2) is computed for significant wave height at the location of three AWAC deployments. Refer to the Appendix for details on how these metrics are computed.

Hindcasted Period	Buoy	Wind	Friction	Whitecapping	N	RMSE	NRMSE	Bias	r2
						m	-	m	-
Autumn 2009	RP09	X	X	X	1416	0.53	0.22	-0.32	0.91
						0.53	0.22	-0.26	0.90
			X			0.53	0.22	-0.27	0.90
		X		X		0.53	0.22	-0.31	0.91
	NP05N	X	X	X	1476	0.47	0.32	-0.40	0.88
						0.44	0.30	-0.37	0.86
			X			0.46	0.31	-0.38	0.86
		X		X		0.46	0.31	-0.39	0.88
Summer 2005	NP05S	X	X	X	666	0.47	0.30	-0.36	0.76
						0.46	0.28	-0.32	0.73
			X			0.46	0.28	-0.33	0.73
		X		X		0.47	0.29	-0.35	0.75
			X	X		0.49	0.30	-0.37	0.73

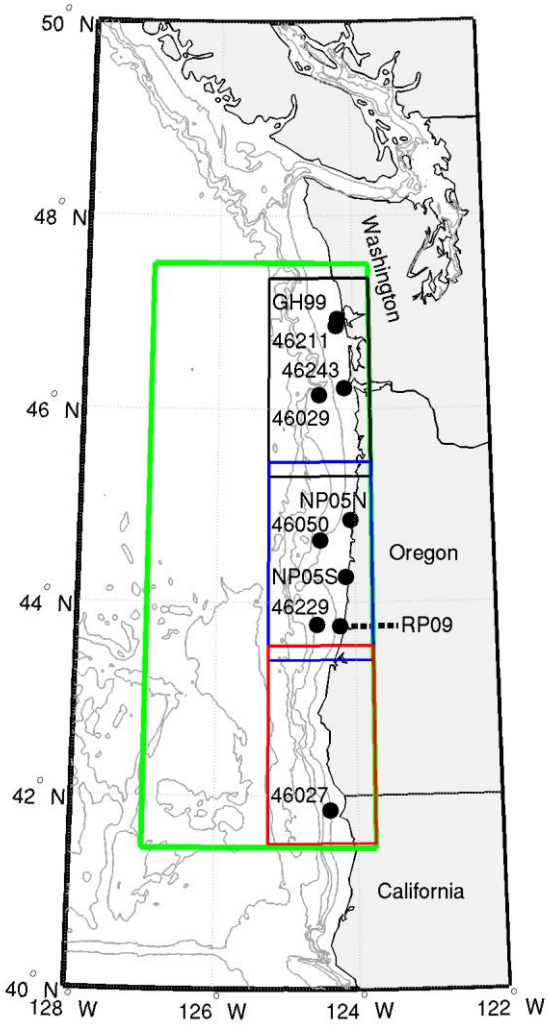

Figure 1: Model Domain. This figure shows the locations (dots) of the data sources used in this study. The Outer Grid is boxed in green, Northern Shelf Grid in black, Central Shelf Grid in blue and Southern Shelf Grid in red. Contours are at 100, 250, 500, 1000, and 3000 meters depth.

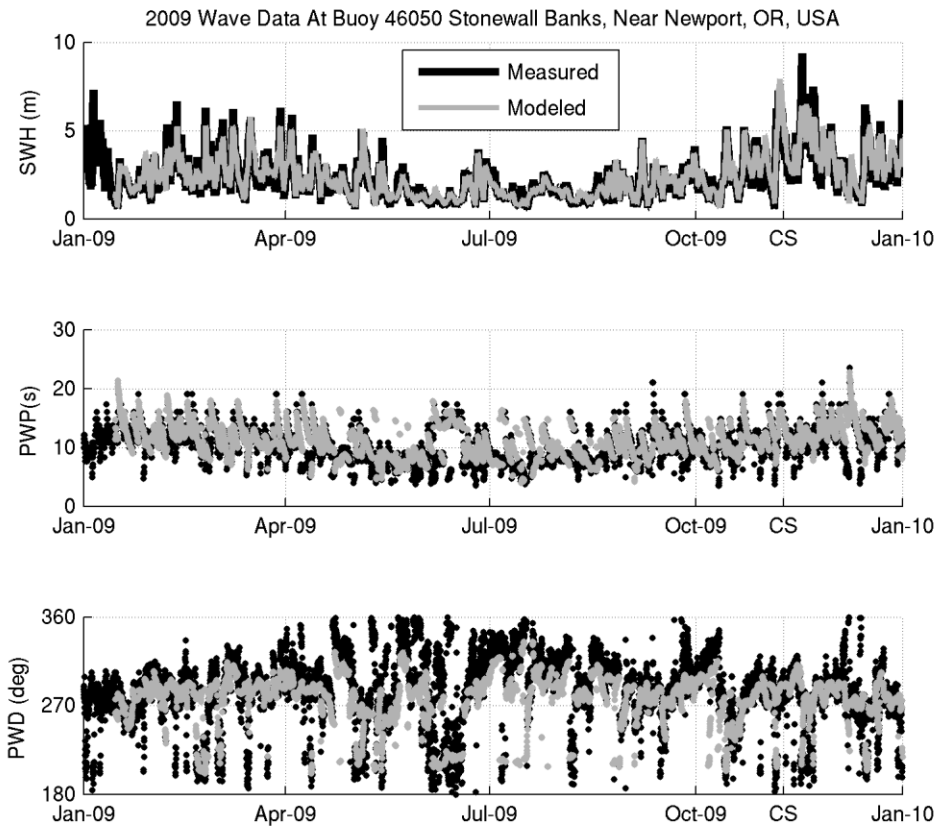

Figure 2: 2009 wave climate at buoy 46050 near Newport, OR, USA. PWP and PWD stand for peak wave period and peak wave direction respectively. PWD is the direction from which the waves approach the buoy, where 360 degrees indicates waves are traveling in the north-south direction. The first two weeks of model spinup were excluded from the plot. CS marks the dates of the discussed 'Case Studies' in Section 2.5.2.

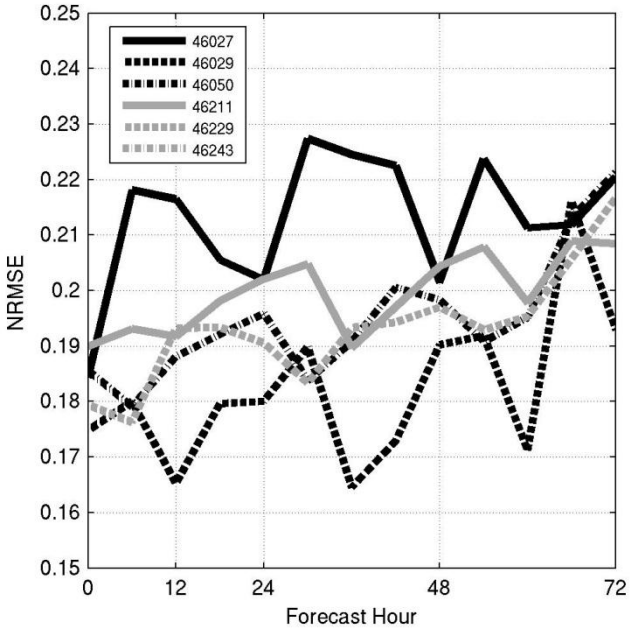

Figure 3: Normalized root-mean-squared errors in significant wave height at selected buoy locations as a function of forecast hour from October to December 2011.

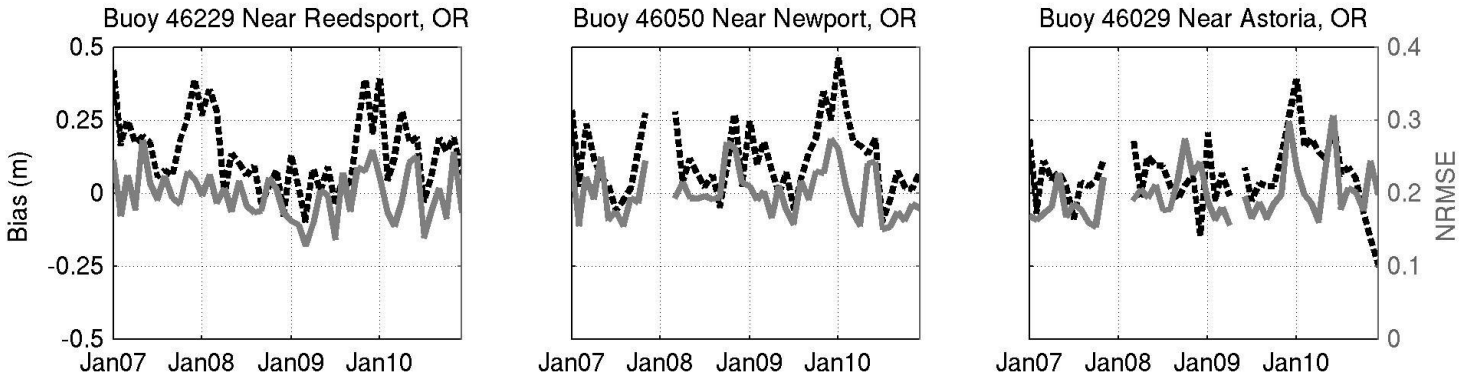

Figure 4: NearWW3_PNW Seasonal Performance. Bias and NRMSE in significant wave height are represented by the black dashed line and gray solid line, respectively. All reported values are averaged over a month from a four year hindcast.

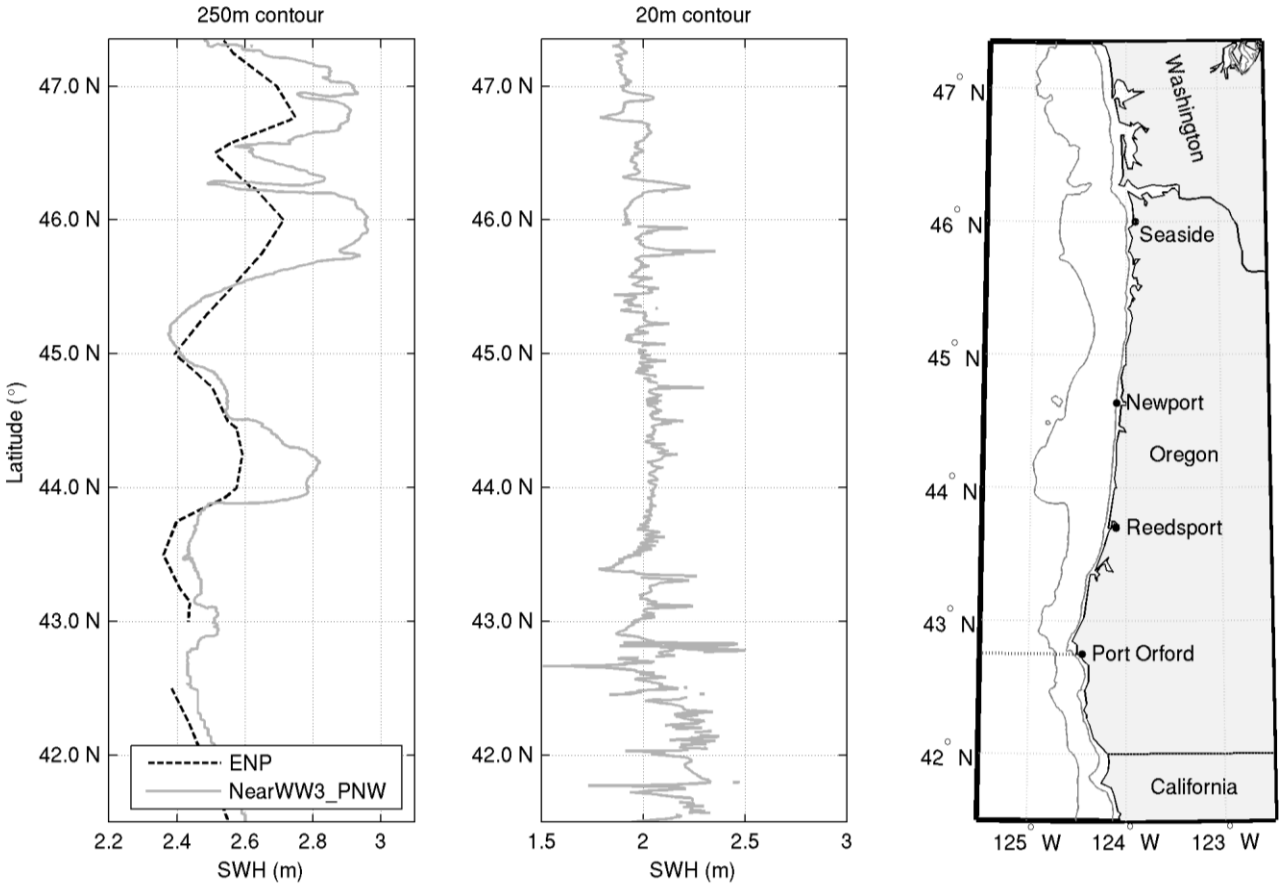

Figure 5: The left panel shows significant wave height interpolated at the 250m contour from both the NearWW3_PNW and NCEP ENP. The center panel shows significant wave height interpolated at the 20m contour. The right panel shows a map of the coast of the study area with contour lines at 20 and 250m water depth. The dotted line at 42.75°N shows the location of Figure 7.

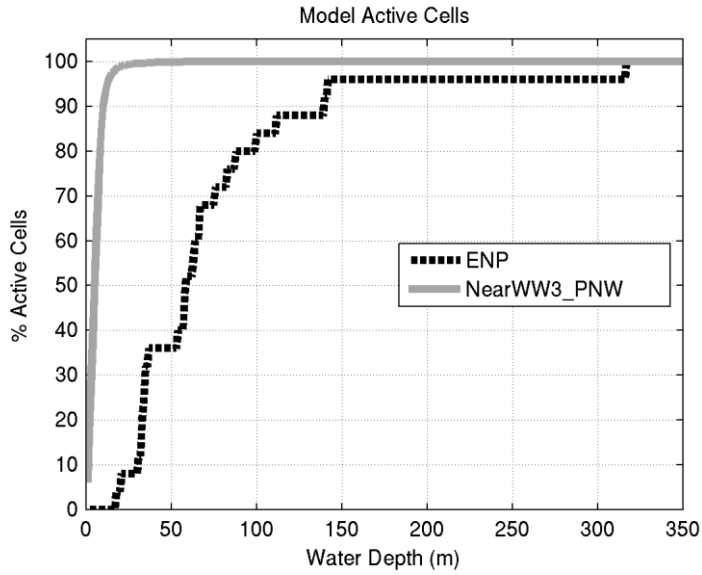

Figure 6: Percentage of alongshore active cells in each model as a function of depth. Only the first active cell in each grid latitude was considered to compute this metric. The ENP has 25 points while NearWW3_PNW has 722 points in the study area.

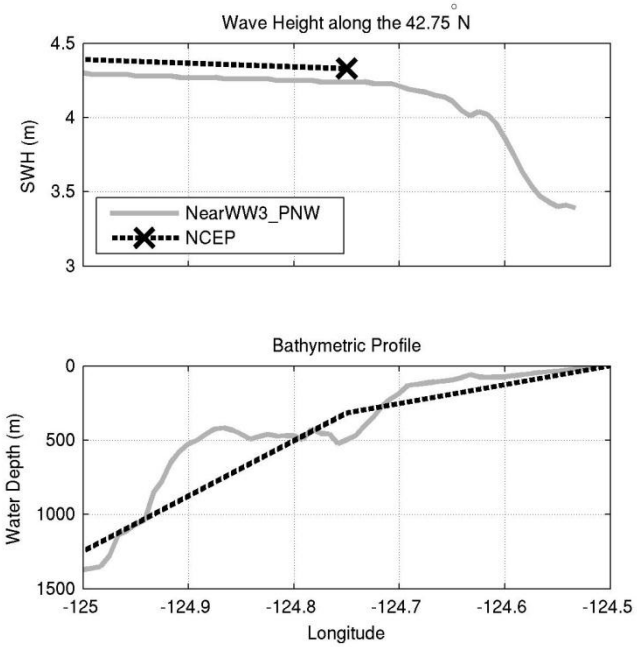

Figure 7: The top panel shows significant wave height along 42.75°N. Forecast data from NCEP and NearPNW_WW3 were used to generate this plot. The NCEP model does not give any information for water depths shallower than 300m while NearPNW_WW3 provides data up to the 20m contour. The bottom panel shows the bathymetries used for the different models.

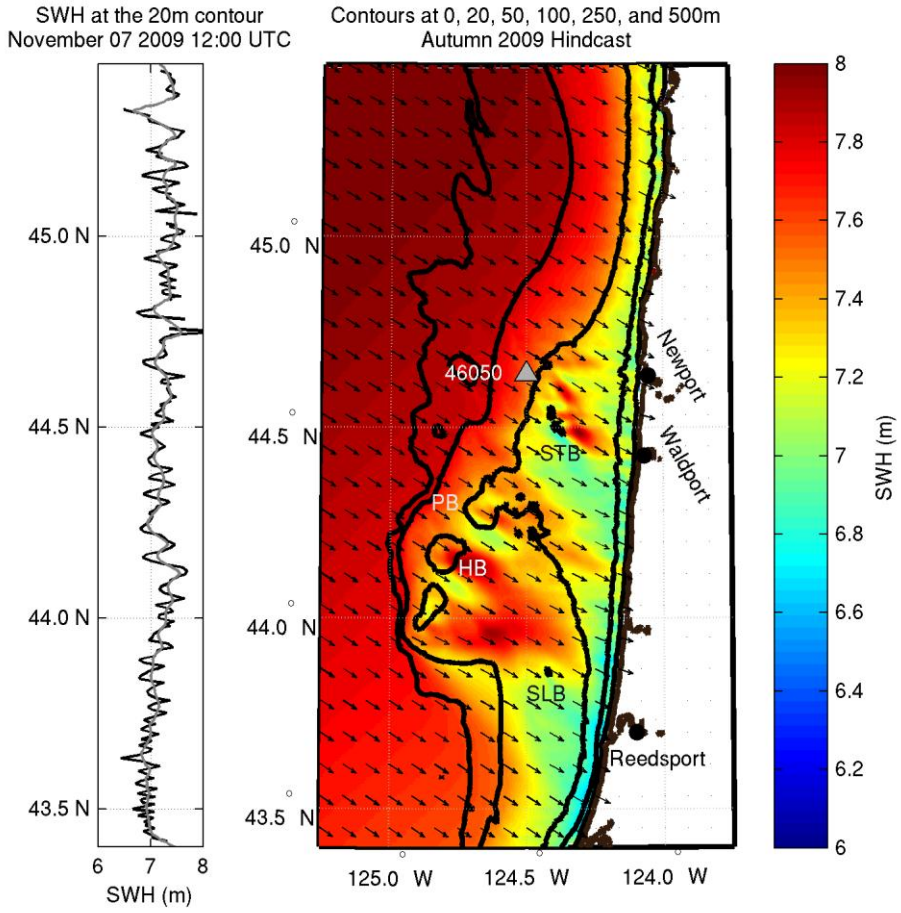

Figure 8: Autumn 2009 NearWW3_PNW Hindcast, wave focusing due to the banks offshore of the central Oregon region. The left panel shows SWH at the 20m contour, both as the model predicts (black) and smoothed using a running average (gray). The right panel shows NearWW3_PNW results at the shelf level. Waves smaller than 6m are masked in the color plot. At buoy 46050 the modeled SWH was 7.6m with mean wave period of 16.3s and peak wave direction of 293°. The banks are shown in the figure STB for Stonewall Banks, PB for Perpetua Bank, HB for Heceta Bank, and SLB for Siltcoos Bank.

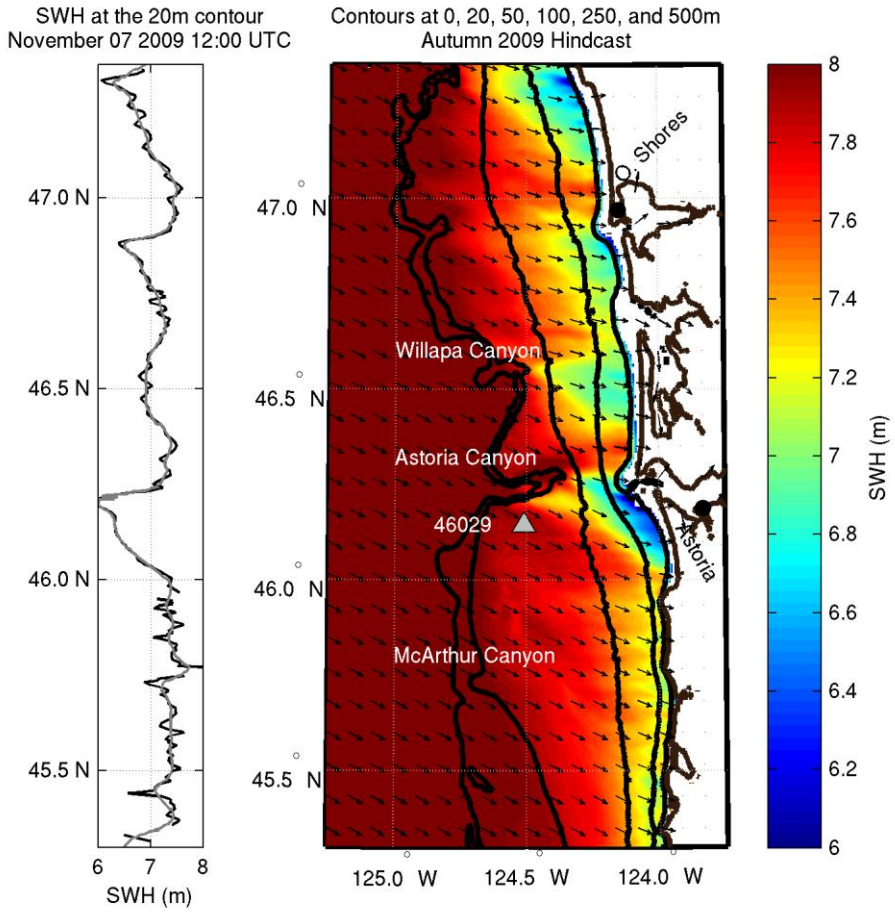

Figure 9: Spatial variations of SWH from the Autumn 2009 NearWW3_PNW hindcast in the northern Oregon and southwestern Washington region. The left panel shows SWH at the 20m contour, both as the model predicts (black) and smoothed using a running average (gray). Large alongshore gradients in wave height are present at the 20m contour. The right panel shows NearWW3_PNW results at the shelf level. Waves smaller than 6m are masked in the color plot. At buoy 46029 the modeled SWH was 7.9m with MWP of 16.4s and PWD of 290°.

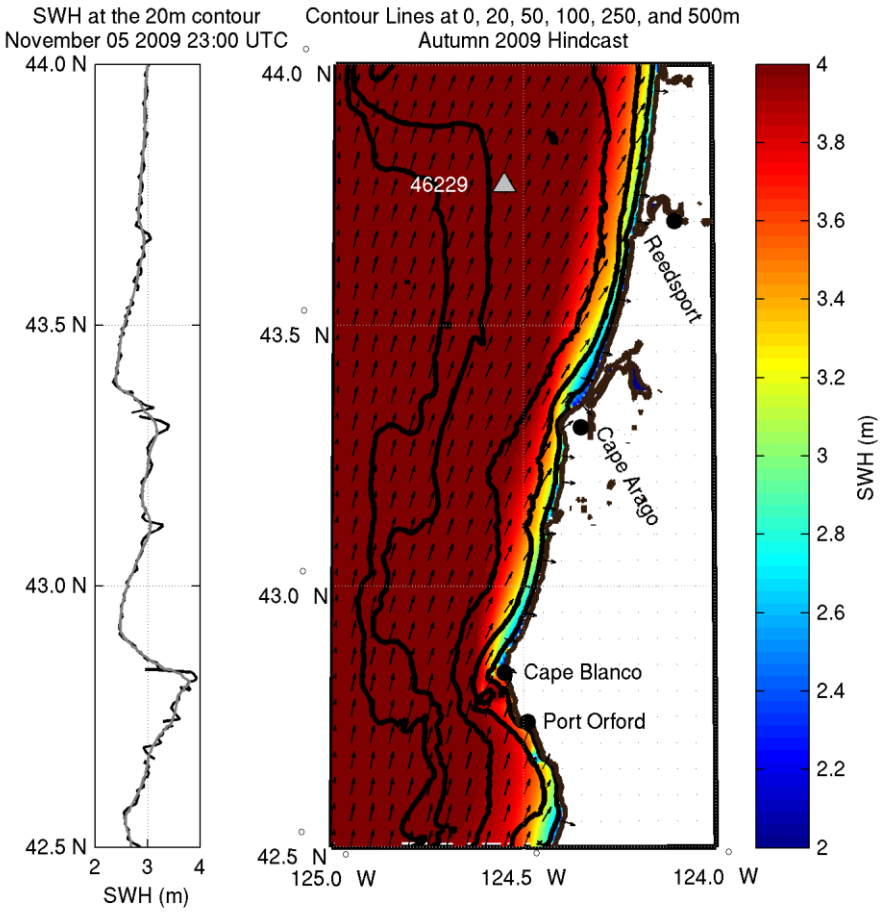

Figure 10: Spatial ariations of SWH from the Autumn 2009 NearWW3_PNW hindcast in the southern Oregon region. The left panel shows SWH at the 20m contour, both as raw model output (black) and smoothed using a running average (gray). The right panel shows NearWW3_PNW results at the shelf level. Wave height reduction is observed north of both Cape Blanco and Cape Arago. At buoy 46229 the modeled SWH was 4.3m with MWP of 8.7s and PWD of 209°.

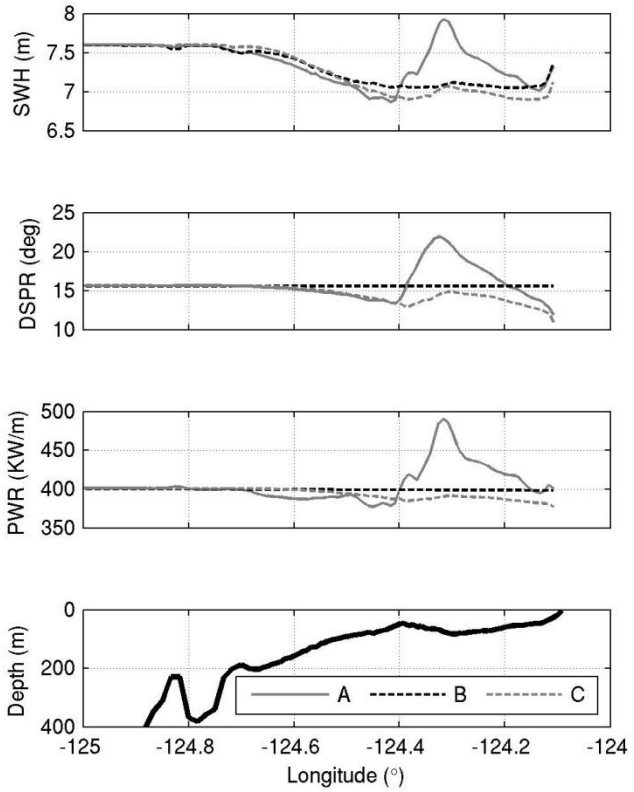

Figure 11: Cross sections along 44.5°N from the SWAN simulations are shown. Case A includes wave refraction. Case B neglects refraction. Case C includes refraction but the simulation was performed for straight and parallel contours on that transect. From top to bottom: significant wave height, directional spread, wave power and local bathymetry. Results at water depth shallower than 20m are masked out since they are not considered in the present discussion. JONSWAP spectral parameters: SWH 7.6m, PWP 16.3s, MWD 293° and directional spread of 12°.

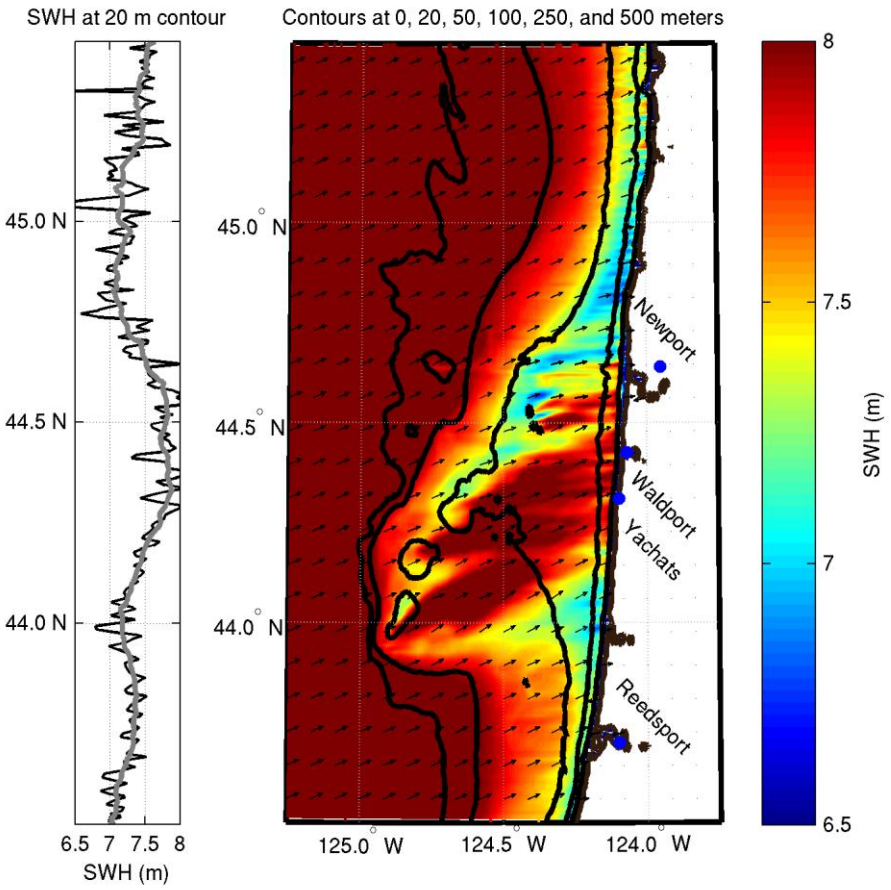

Figure 12: The left panel shows significant wave height at the 20m contour. The black and gray lines show raw model output (unsmoothed) and smoothed with moving averaging, respectively. The right panel shows significant wave height over the modeling domain for a steady-state SWAN simulation. Wave heights are amplified near Waldport, OR. JONSWAP spectral parameters: SWH 8m, PWP 16.3s, and MWD 250°.

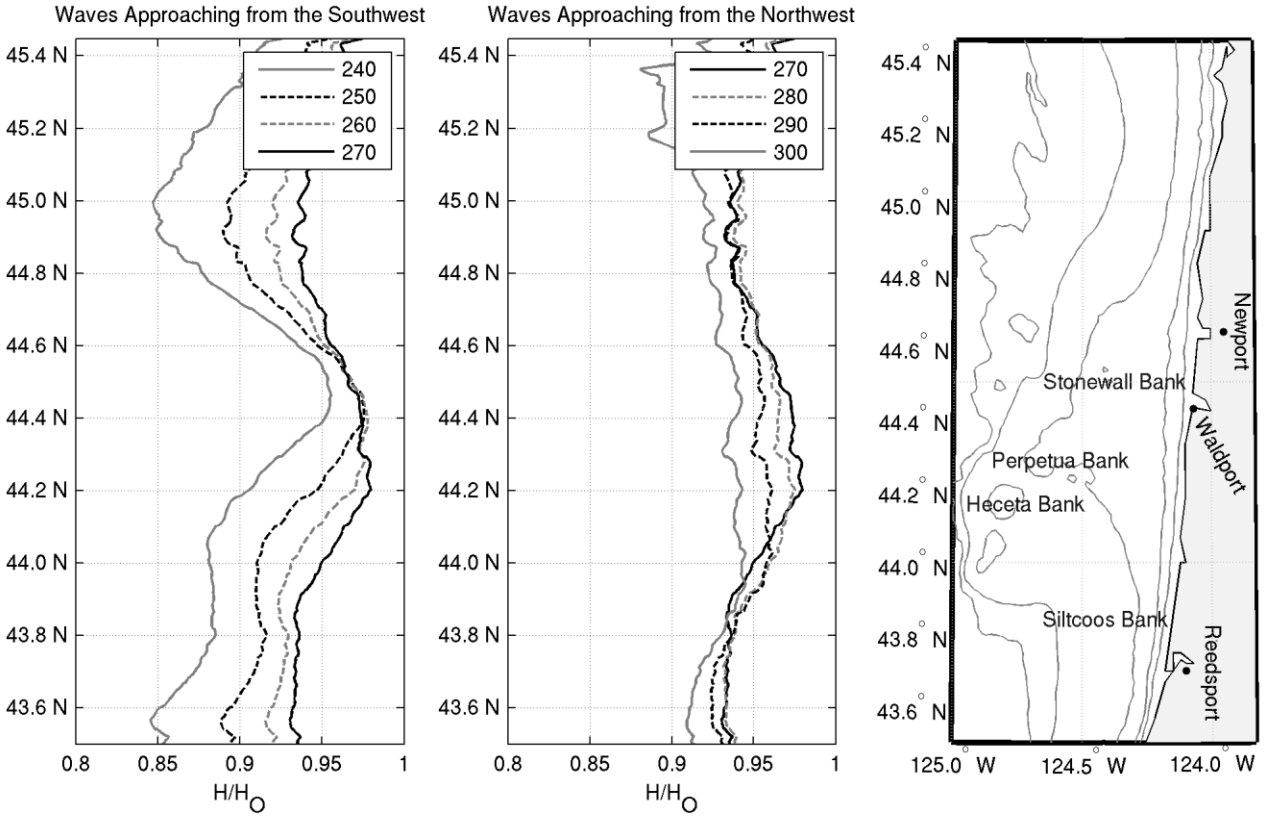

Figure 13: Smoothed wave height normalized by offshore SWH (H_O) is plotted in the left and center panels for different wave incident angles (MWD) at the 20m isobath. The JONSWAP spectrum used for these simulations had a SWH of 8m and PWP of 16.3s. The right panel shows a map of the area considered in these simulations along with the features of interest. Contour lines are drawn at 20, 50, 100, 150 and 250m water depth.

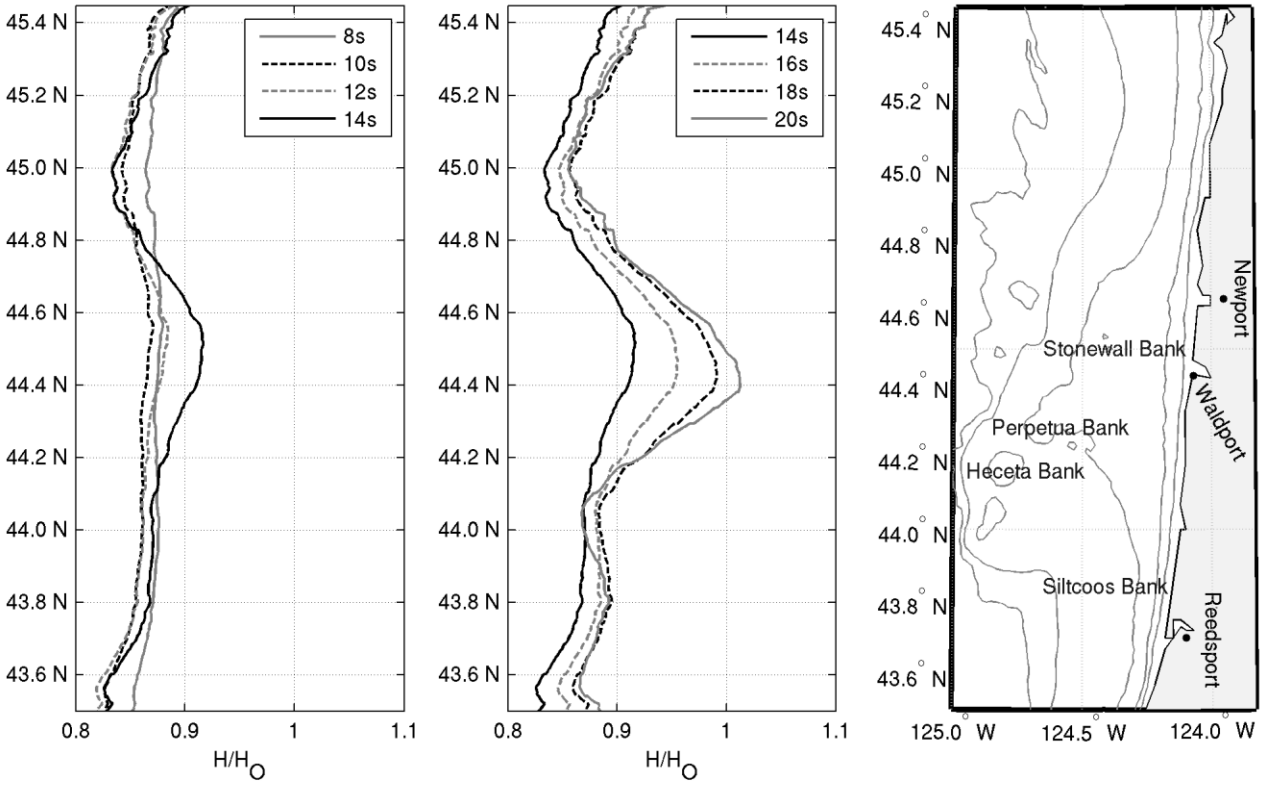

Figure 14: Smoothed wave height normalized by offshore SWH (H_O) is plotted in the left and center panels for different peak wave periods (PWP) at the 20m isobath, wave height gradients are a function of PWP. The JONSWAP spectrum used for these simulations had a SWH of 8m and MWD of 240°. The right panel shows a map of the area considered in these simulations along with the features of interest. Contour lines are drawn at 20, 50, 100, and 250m water depth.

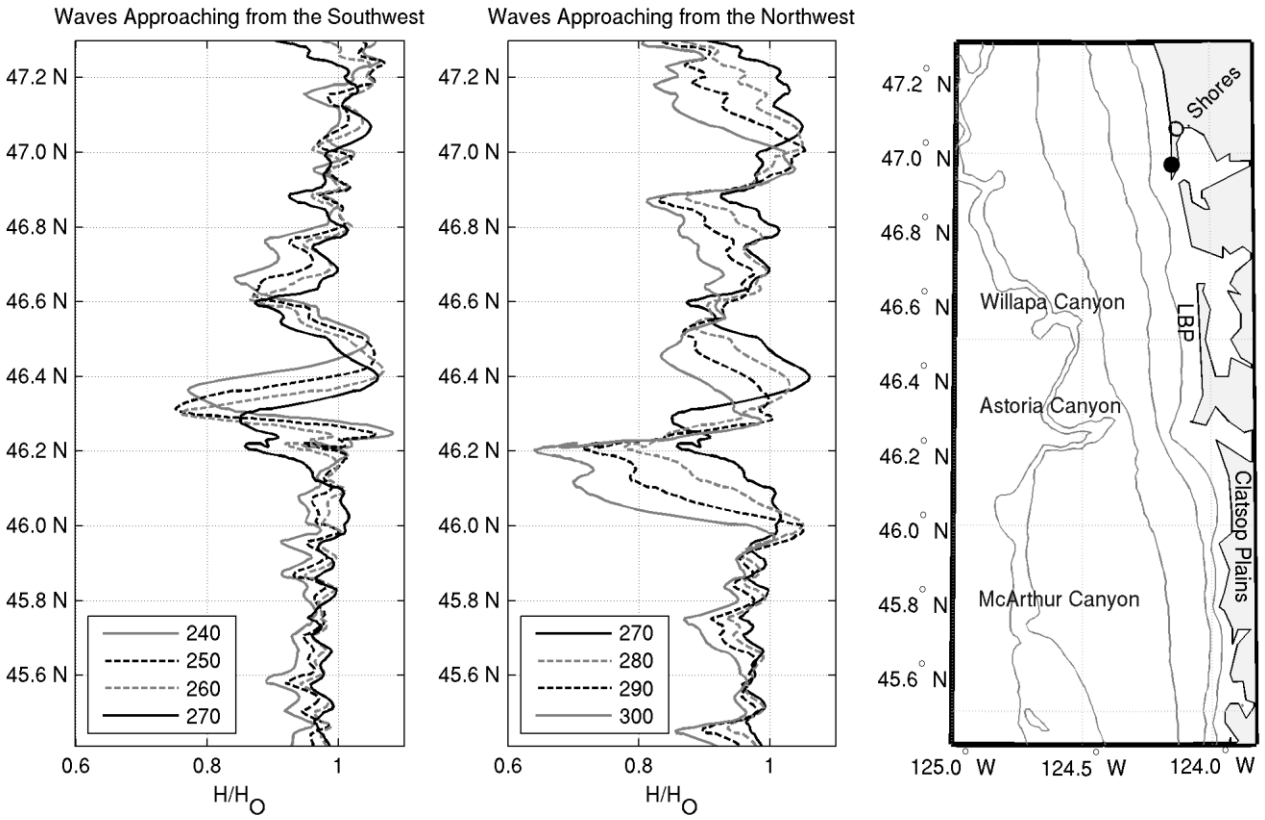

Figure 15: Smoothed wave height normalized by offshore SWH (H_O) is plotted in the left and center plots for different wave incident angles at the 20m isobath in the northern domain. The JONSWAP spectrum used for these simulations had a SWH of 8m and PWP of 18s. The right panel shows a map of the area considered in these simulations along with the features of interest. Contour lines are drawn at 20, 50, 100, 150, and 250m water depth. LBP stands for Long Beach Peninsula.

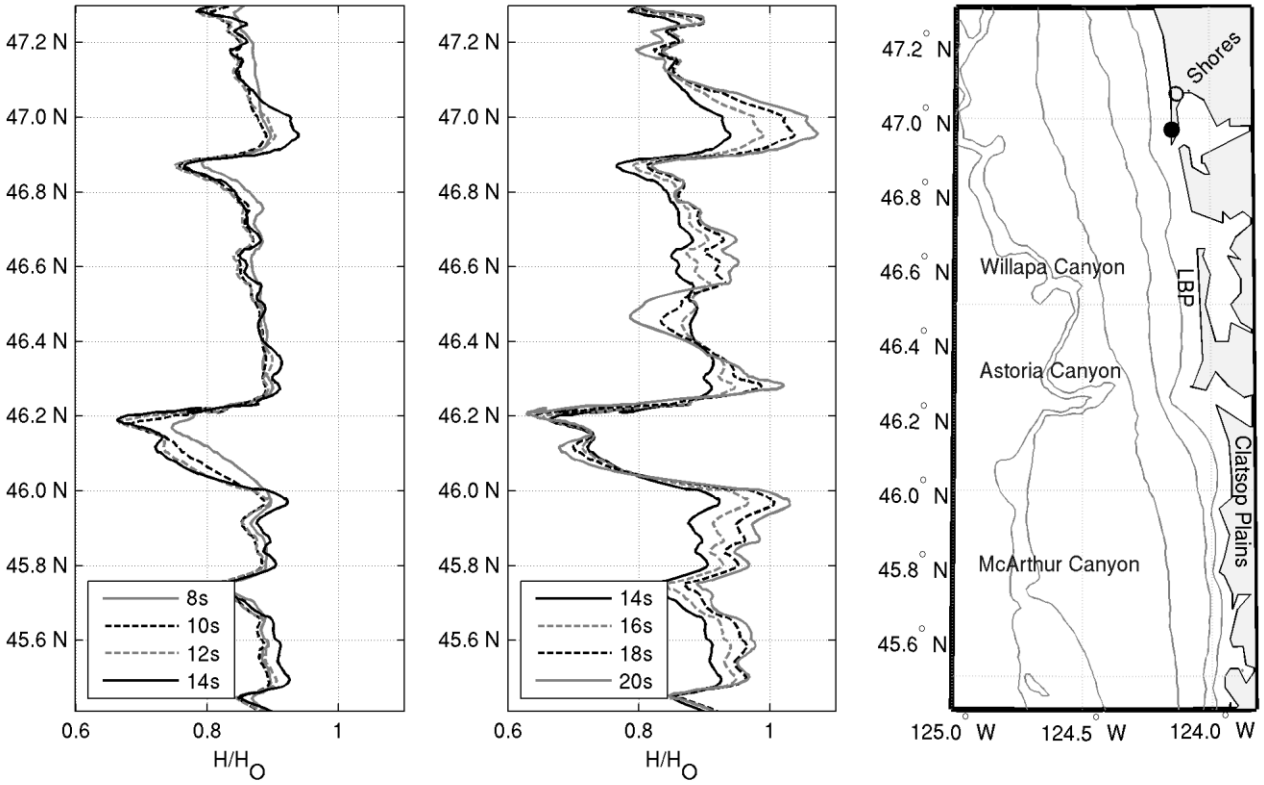

Figure 16: Smoothed wave height normalized by offshore SWH (H_O) as a function of PWP and longitude at the 20m isobaths is plotted in the left and center panels. The JONSWAP spectrum used for these simulations had a SWH of 8m and MWD of 300°. The right panel shows a map of the area considered in these simulations along with the features of interest. Contour lines are drawn at 20, 50, 100, 150, and 250m water depth. LBP stands for Long Beach Peninsula.

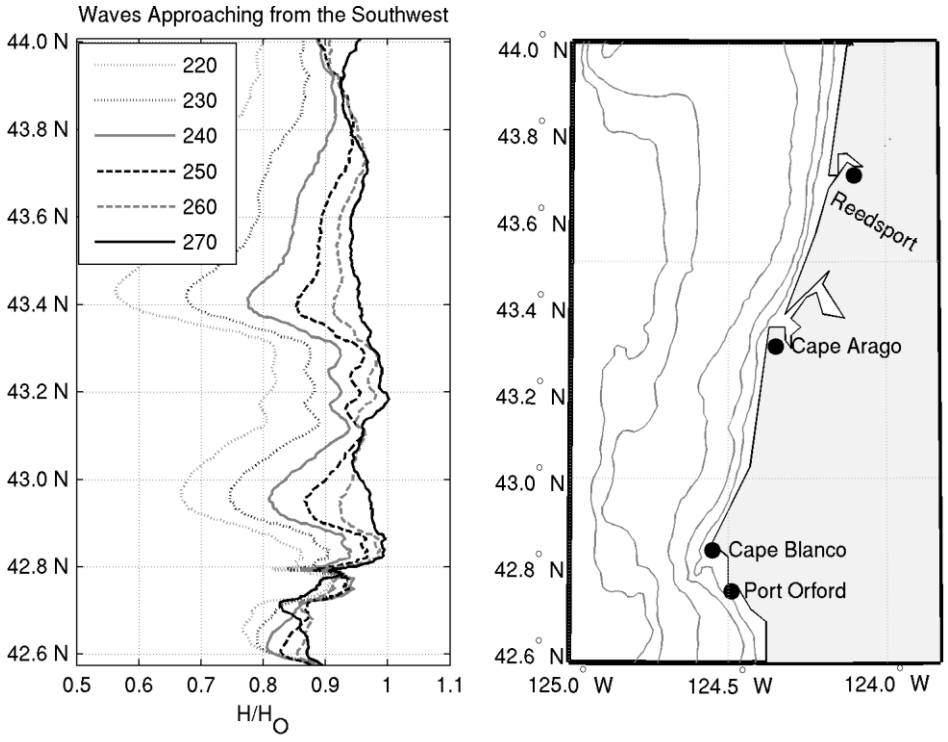

Figure 17: Smoothed wave height normalized by offshore SWH (H_O) as a function of PWD and longitude at the 20m isobath is shown in the left panel. The JONSWAP spectrum used for these simulations had a SWH of 8m and PWP of 18s. The right panel shows a map of the area considered in these simulations along with the features of interest. Contour lines are drawn at 20, 50, 100, 150, and 250m water depth.

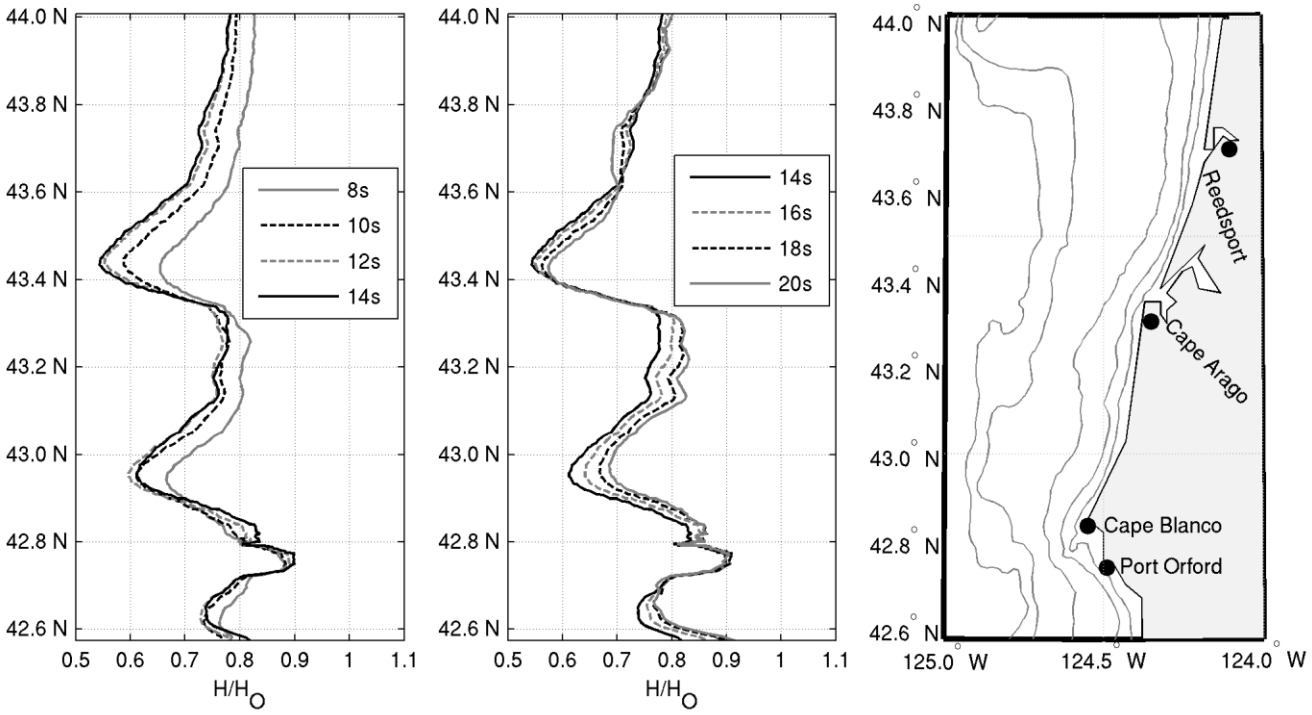

Figure 18: Smoothed wave height normalized by offshore SWH (H_O) as a function of PWP and longitude at the 20m isobath is shown in the left plot. The JONSWAP spectrum used for these simulations had a SWH of 8m and PWD of 220°. The right panel shows a map of the area considered in these simulations along with the features of interest. Contour lines are drawn at 20, 50, 100, 150, and 250m water depth.

3 Concluding Remarks

In this thesis, a recent implementation of a high-resolution localized wave forecasting model for the Oregon and southwest Washington Coasts has been described. This tool advances the prediction capabilities in the region to a point comparable to the State of California; thus, at the moment of this writing providing continuous high quality wave data to a significant portion of the mainland US west coast. In the process, the WAVEWATCH III numerical model, which traditionally has been used to forecast waves in deep water at basin scales, has proven to be a reliable tool to model the wave propagation over the continental shelf. The performance assessment was accomplished by validating the model using *in situ* measurements at intermediate water depths (O(10's m). In addition, a successful collaboration with the NANOOS group has allowed disseminating the data in a user-friendly way. These kinds of tools allow for the evaluation of regional scale coastal behavior and model sensitivity. A series of simulations suggest that neither the inclusion of bottom friction nor wind input at the shelf scale level provide significant differences in the model accuracy for long term forecasting and hindcasting. In addition, a careful evaluation of the wave propagation over the shelf suggests that the major bathymetric features in the area are capable of influencing the wave field in the nearshore. This is accomplished mostly by the process of refraction, where waves react to these features (e.g. canyons, banks, capes, etc.) in the offshore by focusing and defocussing in certain regions generating significant alongshore gradients in the wave field.

References

Allan, J. C., Komar, P. D., 2000. Are ocean wave heights increasing in the Eastern North Pacific? Transaction of the American Geophysical Union 81 (47), 561-567.

Allan, J. C., Komar, P. D., 2002. Extreme storms on the Pacific Northwest coast during the 1997-98 El Niño and 1998-99 La Niña. Journal of coastal research 18 (1), 175-193.

Allan, J. C., Komar, P. D., 2006. Climate controls on US west coast erosion processes. Journal of Coastal Research 223, 511-529.

Alvarez-Ellacuria, A., Orfila, A., Olabarrieta, M., Medina, R., Vizoso, G., Tintoré, J., 2010. A nearshore wave and current operational forecasting system. Journal of Coastal Research 263, 503_509.

Amante, C., Eakins, B. W., 2009. ETOPO1 1 Arc-Minute global relief model: Procedures, data sources and analysis. NOAA Technical Memorandum NESDIS NGDC-24.

Arinaga, R. A., Cheung, K. F., 2012. Atlas of global wave energy from 10 years of reanalysis and hindcast data. Renewable Energy 39 (1), 49-64.

Astoria Canyon, 2012. Encyclopaedia britannica online. Retrieved 10 April, 2012. URL http://www.britannica.com/EBchecked/topic/39897/Astoria-Canyon

Battjes, J. A., Janssen, J. P. F. M., 1978. Energy loss and set-up due to breaking of random waves. In: 16th International Conference on Coastal Engineering. ASCE, Hamburg, Germany, pp. 569-587.

Booij, N., Holthuijsen, L. H., 1987. Propagation of ocean waves in discrete spectral wave models. Journal of Computational Physics 68 (2), 307-326.

Booij, N., Ris, R. C., Holthuijsen, L. H., 1999. A third-generation wave model for coastal regions 1. Model description and validation. Journal of Geophysical Research 104 (C4), PP. 7649-7666.

Carignan, K. S., Taylor, L. A., Eakins, B. W., Warnken, R. R., 2009a. Digital elevation model of Astoria, Oregon: Procedures, data sources and analysis. NOAA Technical Memorandum NESDIS NGDC-22, National Geophysical Data Center, Boulder, Colorado.

Carignan, K. S., Taylor, L. A., Eakins, B.W., Warnken, R. R., Lim, E., Grothe, P., 2009b. Digital elevation model of central Oregon coast: Procedures, data sources and analysis. NOAA Technical Memorandum NESDIS NGDC-25, National Geophysical Data Center, Boulder, Colorado.

Carignan, K. S., Taylor, L. A., Eakins, B. W., Warnken, R. R., Sazonova, T., Schoolcraft, D. C., 2009c. Digital elevation model of Garibaldi, Oregon: Procedures, data sources and analysis. NOAA Technical Memorandum NESDIS NGDC-16, National Geophysical Data Center, Boulder, Colorado.

Carignan, K. S., Taylor, L. A., Eakins, B. W., Warnken, R. R., Sazonova, T., Schoolcraft, D. C., 2009d. Digital elevation model of Port Orford, Oregon: Procedures, data sources and analysis. NOAA Technical Memorandum NESDIS NGDC-21, National Geophysical Data Center, Boulder, Colorado.

Christensen, A., Rowe, S., Needham, M. D., 2007. Value orientations, awareness of consequences, and participation in a whale watching education program in oregon. Human Dimensions of Wildlife 12 (4), 289-293.

Cornett, A. M., 2009. A global wave energy resource assessment. Sea Technology 50 (4), 59-64.

Dean, R. G., Dalrymple, R. A., 1991.Water wave mechanics for engineers and scientists. Vol. 2 of Advanced Series on Ocean Engineering. World Scientific.

Environmental Modeling Center, 2003. The GFS atmospheric model. NCEP Ofice Note 442, NOAA / NWS / NCEP, 14 pp.

Falcão, A. F. d. O., 2010. Wave energy utilization: A review of the technologies. Renewable and Sustainable Energy Reviews 14 (3), 899-918.

Folley, M., Whittaker, T., 2009. Analysis of the nearshore wave energy resource. Renewable Energy 34 (7), 1709-1715.

Gelfenbaum, G., Sherwood, C. R., Kerr, L. A., Kurrus, K., 2000. Grays harbor wave refraction experiment 1999: Data report. Open-File Report 00-404, USGS.

Gemmrich, J., Thomas, B., Bouchard, R., 2011. Observational changes and trends in Northeast Pacific wave records. Geophysical Research Letters 38, 5 pp.

Gorrell, L., Raubenheimer, B., Elgar, S., Guza, R., 2011. SWAN predictions of waves observed in shallow water onshore of complex bathymetry. Coastal Engineering 58 (6), 510-516.

Grothe, P., Taylor, L. A., Eakins, B. W., Carignan, K. S., Caldwell, R. J., Lim, E., Friday, D. Z., 2011. Digital elevation model of Crescent City, California: Procedures, data sources and analysis. NOAA Technical Memorandum NESDIS NGDC-51, National Geophysical Data Center, Boulder, Colorado.

Grothe, P., Taylor, L. A., Eakins, B. W., Carignan, K. S., Warnken, R. R., Lim, E., Caldwell, R. J., 2010. Digital elevation model of Taholah, Washington: Procedures, data sources and analysis. NOAA Technical Memorandum NESDIS NGDC-34, National Geophysical Data Center, Boulder, Colorado.

Hanson, J. L., B. A. Tracy, H. L. Tolman and R. D. Scott, 2009. Pacific hindcast performance of three numerical models. Journal of Atmospheric and Oceanic Technology 26 (8), 1614-1633.

Hasselmann, K., Barnett, T. P., Bouws, E., Carlson, H., Cartwright, D. E., Enke, K., Ewing, J. A., Gienapp, H., Hasselmann, D. E., Kruseman, P., Meerburg, A., Mueller, P., Olbers, D. J., Richter, K., Sell, W., Walden, H., 1973. Measurements of wind-wave growth and swell decay during the joint north sea wave project (JONSWAP). Ergaenzungsheft zur Deutschen Hydrographischen Zeitschrift A (12), 95pp.

Hasselmann, S., Hasselmann, K., Allender, J. H., Barnett, T. P., 1985. Computations and parameterizations of the nonlinear energy transfer in a gravity-wave specturm. part II: parameterizations of the nonlinear energy transfer for application in wave models. Journal of Physical Oceanography 15, 1378-1391.

Iversen, H. W., 1952. Waves and breakers in shoaling water. Proceedings of the International Conference on Coastal Engineering 1 (3), 1-12.

Kirincich, A. R., Lentz, S. J., Barth, J. A., 2009. Wave-Driven Inner-Shelf motions on the Oregon coast*. Journal of Physical Oceanography 39 (11), 2942-2956.

Komar, P. D., Allan, J. C., Ruggiero, P., 2009. Ocean wave climates: trends and variations due to Earth's changing climate. In: Kim, Y. C. (Ed.), Handbook of Coastal and Ocean Engineering. World Scientific Publishing Co, 971-975.

Lenee-Bluhm, P., Paasch, R., Özkan-Haller, H. T., 2011. Characterizing the wave energy resource of the US pacific northwest. Renewable Energy 36 (8), 2106-2119.

Long, J. W., Özkan-Haller, H. T., 2005. Offshore controls on nearshore rip currents. Journal of Geophysical Research 110, 21 pp.

Menéndez, M., Méndez, F. J., Losada, I. J., Graham, N. E., 2008. Variability of extreme wave heights in the northeast Pacific Ocean based on buoy measurements. Geophysical Research Letters 35, 6 pp.

NDBC, 2009: NDBC Technical Document 09-02, Handbook of automated data quality control checks and procedures. NOAA National Data Buoy Center, 78 pp.

Oregon Wave Energy Trust (OWET). http://www.oregonwave.org/about/ (accessed August 2, 2012).

Rao, S., Mandal, S., 2005. Hindcasting of storm waves using neural networks. Ocean Engineering 32 (5-6), 667-684.

Risien, C. M., Allan, J. C., Blair, R., Jaramillo, A. V., Jones, D., Kosro, P.M., Martin, D., Mayora, E., Newton, J.A., Tanner, T., Uczekaj, S. A., 2009. The NANOOS Visualization System: Aggregating, displaying and serving data. OCEANS 2009, MTS/IEEE Biolxi – Marine Technology for out future: global and local challenges, 1-9.

Rogers, W. E., Kaihatu, J. M., Hsu, L., Jensen, R. E., Dykes, J. D., Holland, K. T., 2007. Forecasting and hindcasting waves with the SWAN model in the southern California bight. Coastal Engineering 54 (1), 1-15.

Ruggiero, P., Komar, P. D., Allan, J. C., 2010. Increasing wave heights and extreme value projections: The wave climate of the U.S. Pacific northwest. Coastal Engineering 57 (5), 539-552.

Sela, J. G., 1980. Spectral modeling at the National Meteorological Center. MonthlyWeather Review 108 (9), 1279-1292.

Seymour, R. J., 2011. Evidence for changes to the northeast Pacific wave climate. Journal of Coastal Research 27, 194-201.

Stockdon, H. F., Holman, R. A., Howd, P. A., Sallenger Jr., A. H., 2006. Empirical parameterization of setup, swash, and runup. Coastal Engineering 53 (7), 573-588.

Tolman, H. L., Jun. 2002a. Alleviating the garden sprinkler effect in wind wave models. Ocean Modelling 4 (3-4), 269-289.

Tolman, H. L., 2002b. Validation of WAVEWATCH III version 1.15 for a global domain. NOAA / NWS / NCEP / OMB (Nr. 213), 33 pp.

Tolman, H. L., 2006. Development of a multi-grid version of WAVEWATCH III. Tech. Rep. 256, NOAA/NWS/NCEP/MMAB.

Tolman, H. L., 2008. A mosaic approach to wind wave modeling. Ocean Modelling 25 (1-2), 35-47.

Tolman, H. L., Chalikov, D., 1996. Source terms in a Third-Generation wind wave model. Journal of Physical Oceanography 26 (11), 2497-2518.

Young, I. R., Zieger, S., Babanin, A. V., 2011. Global trends in wind speed and wave height. Science 332 (6028), 451-455.

APPENDIX

Appendix Statistical Metrics

In the following statistical metrics, N represents the number of observations. $MEAS$ and EST are the measured and modeled values. These metrics are root-mean-squared error (RMSE)

$$RMSE = \sqrt{\frac{\sum(MEAS - EST)^2}{N}}; \tag{A1}$$

normalized root-mean-squared error (NRMSE)

$$NRMSE = \sqrt{\frac{1}{N}\sum\left(\frac{MEAS - EST}{MEAS}\right)^2}; \tag{A2}$$

bias

$$Bias = \frac{1}{N}\sum EST - MEAS; \tag{A3}$$

and linear correlation coefficient (r2)

$$r2 = \frac{[\sum(MEAS_i - \overline{MEAS})(EST_i - \overline{EST})]^2}{\sqrt{(\sum(MEAS_i - \overline{MEAS})^2)(\sum(EST_i - \overline{EST})^2)}} \tag{A4}$$

A perfect model run with respect to measured data will report a RMSE, NRMSE, and bias of zero and a linear correlation coefficient of 1. These statistics are computed only where data and model coincide in time allowing for a 10 minute offset.